

# The $\Upsilon$ and $\Upsilon'$ Leptonic Widths, $a_\mu^b$ and $m_b$ from full lattice QCD

B. Colquhoun,<sup>1</sup> R. J. Dowdall,<sup>2</sup> C. T. H. Davies,<sup>1,\*</sup> K. Hornbostel,<sup>3</sup> and G. P. Lepage<sup>4</sup>  
(HPQCD collaboration)<sup>†</sup>

<sup>1</sup>*SUPA, School of Physics and Astronomy, University of Glasgow, Glasgow, G12 8QQ, UK*

<sup>2</sup>*DAMTP, University of Cambridge, Wilberforce Road, Cambridge, CB3 0WA, UK*

<sup>3</sup>*Southern Methodist University, Dallas, Texas 75275, USA*

<sup>4</sup>*Laboratory of Elementary-Particle Physics, Cornell University, Ithaca, New York 14853, USA*

(Dated: October 7, 2018)

We determine the decay rate to leptons of the ground-state  $\Upsilon$  meson and its first radial excitation in lattice QCD for the first time. We use radiatively-improved NRQCD for the  $b$  quarks and include  $u$ ,  $d$ ,  $s$  and  $c$  quarks in the sea with  $u/d$  masses down to their physical values. We find  $\Gamma(\Upsilon \rightarrow e^+e^-) = 1.19(11)$  keV and  $\Gamma(\Upsilon' \rightarrow e^+e^-) = 0.69(9)$  keV, both in good agreement with experiment. The decay constants we obtain are included in a summary plot of meson decay constants from lattice QCD given in the Conclusions. We also test time-moments of the vector current-current correlator against values determined from the  $b$  quark contribution to  $\sigma(e^+e^- \rightarrow \text{hadrons})$  and calculate the  $b$ -quark piece of the hadronic vacuum polarisation contribution to the anomalous magnetic moment of the muon,  $a_\mu^b = 0.271(37) \times 10^{-10}$ . Finally we determine the  $b$ -quark mass, obtaining in the  $\overline{MS}$  scheme,  $\overline{m}_b(\overline{m}_b, n_f = 5) = 4.196(23)$  GeV, the most accurate result from lattice QCD to date.

## I. INTRODUCTION

Precision tests of lattice QCD against experiment are critical to provide benchmarks against which to calibrate the reliability of predictions from lattice QCD for masses and matrix elements [1]. Weak decay matrix elements calculated in lattice QCD, for example, are critical to the flavor physics programme [2, 3] of over-determining the Cabibbo-Kobayashi-Maskawa (CKM) matrix to find signs of new physics. This is particularly important for mesons containing a valence  $b$  quark. Lattice QCD therefore needs to provide a range of results for a variety of hadrons containing  $b$  quarks to make sure that the analysis of systematic errors is sound. Focussing on quantities that are well measured experimentally enables strong tests to be made.

Here we give lattice QCD results for the electromagnetic annihilation rate for mesons, the  $\Upsilon$  and its radial excitation the  $\Upsilon'$ , containing valence  $b$  quarks and antiquarks. The hadronic parameter that determines this rate, the matrix element of the vector current between the vacuum and the  $\Upsilon$ , is parameterised by a quantity known as the decay constant. The determination of this intrinsically non-perturbative quantity is both a test of our lattice QCD approach to  $b$  quark physics and a test of QCD itself, since other methods of determining this rate have large systematic errors or uncertainties from model-dependence that reduce the significance of the comparison with experiment (see, for example, the discussion in [4–7]). The recent success of lattice QCD in determining the leptonic width of the  $J/\psi$  to 4% [8, 9] makes clear the power of a model-independent nonperturbative ap-

proach to such calculations and we apply that approach here, for the first time doing a complete calculation. For related earlier work in Lattice QCD see [10–12]. This calculation also provides the ‘missing piece’ of a set of determinations of decay constants for a range of mesons by the HPQCD collaboration and others. We provide a plot which summarises the results.

Another test against experiment that can be done with the same correlation functions is that of the  $b$  quark contribution to  $\sigma(e^+e^- \rightarrow \text{hadrons})$ . Again this is an electromagnetic rate and so the comparison is free from CKM uncertainties. Here we also build on the success of a similar calculation of the  $c$  quark contribution [8].

Finally we determine the  $b$  quark mass using the current-current correlator method [13, 14]. Since we use the NonRelativistic QCD (NRQCD) approach to  $b$  quarks [15] here (including now  $\mathcal{O}(\alpha_s)$  corrections to non-leading terms in the nonrelativistic expansion [16]) our result for  $m_b$  has very different systematic errors to that from the relativistic Highly Improved Staggered Quark (HISQ) formalism [14]. Since both determinations have 0.5% uncertainties this provides a very stringent comparison. We can also compare our result to that obtained using an NRQCD calculation of  $\Upsilon$  binding energies coupled with a lattice QCD perturbation theory calculation of the NRQCD zero of energy [17]. The agreement of these three very different determinations is a good test of our control of systematic errors. Accurate determination of the  $b$  quark mass is important for calculation of the expected Higgs branching fraction to  $b\bar{b}$  [18, 19].

The paper is laid out as follows: Section II gives an overview of the methods used in the lattice calculation and then Section III gives each set of results in turn, with additional details in Appendices B and A. Section IV gives our conclusions, including a summary of lattice QCD results for meson decay constants.

\*christine.davies@glasgow.ac.uk

†URL: <http://www.physics.gla.ac.uk/HPQCD>

## II. LATTICE CALCULATION

We use ensembles of lattice gluon configurations provided by the MILC collaboration [20] at values of the lattice spacing,  $a \approx 0.15$  fm, 0.12 fm and 0.09 fm. The configurations include the effect of  $u$ ,  $d$ ,  $s$  and  $c$  quarks in the sea using the highly improved staggered quark (HISQ) formalism [21] and a gluon action improved through  $\mathcal{O}(\alpha_s a^2)$  [22]. These then give significant improvements in the control of systematic errors from finite lattice spacing and light quark mass effects over earlier configurations.

We work at two different values of the  $u/d$  quark masses (which are taken to be degenerate) in the sea. One is at one fifth of the  $s$  quark mass, the other is the physical  $u/d$  quark mass ( $m_s/27.5$ ). The lattice spacing on these configurations is determined from the mass difference between the  $\Upsilon'$  and the  $\Upsilon$  [16]. Table I lists the parameters of the ensembles.

### A. NRQCD

On these configurations we calculate  $b$  quark propagators using the improved NRQCD action developed in [16] and [23]. The NRQCD Hamiltonian we use is given by:

$$\begin{aligned}
 aH &= aH_0 + a\delta H; \\
 aH_0 &= -\frac{\Delta^{(2)}}{2am_b}, \\
 a\delta H &= -c_1 \frac{(\Delta^{(2)})^2}{8(am_b)^3} + c_2 \frac{i}{8(am_b)^2} \left( \nabla \cdot \tilde{\mathbf{E}} - \tilde{\mathbf{E}} \cdot \nabla \right) \\
 &\quad - c_3 \frac{1}{8(am_b)^2} \sigma \cdot \left( \tilde{\nabla} \times \tilde{\mathbf{E}} - \tilde{\mathbf{E}} \times \tilde{\nabla} \right) \\
 &\quad - c_4 \frac{1}{2am_b} \sigma \cdot \tilde{\mathbf{B}} + c_5 \frac{\Delta^{(4)}}{24am_b} \\
 &\quad - c_6 \frac{(\Delta^{(2)})^2}{16n_h(am_b)^2}. \tag{1}
 \end{aligned}$$

Here  $\nabla$  is the symmetric lattice derivative and  $\Delta^{(2)}$  and  $\Delta^{(4)}$  the lattice discretization of the continuum  $\sum_i D_i^2$  and  $\sum_i D_i^4$  respectively.  $am_b$  is the bare  $b$  quark mass in units of the lattice spacing. The parameter  $n_h$  will be discussed below.  $\tilde{\mathbf{E}}$  and  $\tilde{\mathbf{B}}$  are the chromoelectric and chromomagnetic fields calculated from an improved clover term [12]. The  $\tilde{\mathbf{B}}$  and  $\tilde{\mathbf{E}}$  are made anti-hermitian but not explicitly traceless, to match the perturbative calculations done using this action.

In terms of an expansion in the velocity of the heavy quark,  $v$ ,  $H_0$  is  $\mathcal{O}(v^2)$  and  $\delta H$  is  $\mathcal{O}(v^4)$ , including discretisation corrections.  $H_0$  contains the bare quark mass parameter which is nonperturbatively tuned to the correct value for the  $b$  quark as discussed below. The terms in  $\delta H$  have coefficients  $c_i$  whose values are fixed from matching lattice NRQCD to full QCD. This matching takes account of high momentum modes that differ be-

Set	$a/\text{fm}$	$am_l$	$am_s$	$am_c$	$L_s/a$	$L_t/a$	$N_{\text{cfg}}$
1	0.1474(5)(14)	0.013	0.065	0.838	16	48	1020
2	0.1450(3)(14)	0.00235	0.0647	0.831	32	48	1000
3	0.1219(2)(9)	0.0102	0.0509	0.635	24	64	1052
4	0.1189(2)(9)	0.00184	0.0507	0.628	48	64	1000
5	0.0884(3)(5)	0.0074	0.037	0.440	32	96	1008

TABLE I: Details of gluon field configurations used in this calculation [20].  $a$  is the lattice spacing, fixed from the mass difference between the  $\Upsilon'$  and  $\Upsilon$  in [16]. The first error is from statistics and the second from NRQCD systematics in that determination and from experiment. Sets 1 and 2 are ‘very coarse’, sets 3 and 4 are ‘coarse’ and set 5 is ‘fine’.  $am_l$ ,  $am_s$  and  $am_c$  are the light ( $u$  and  $d$  are taken to have the same mass), strange and charm sea quark masses. Sets 1, 3 and 5 have  $m_l = 0.2m_s$  and sets 2 and 4 have  $m_l$  at its physical value.  $L_s/a$  and  $L_t/a$  are the number of lattice sites in the spatial and temporal directions respectively and  $N_{\text{cfg}}$  is the number of configurations in the ensemble. We calculate propagators from 4 or 16 time sources on each ensemble to increase statistics. Correlators are calculated up to a time separation between source and sink of 40 on sets 1–4 and 48 on fine set 5.

tween NRQCD and full QCD and so it can be done perturbatively, giving the  $c_i$  the expansion  $1 + c_i^{(1)}\alpha_s + \mathcal{O}(\alpha_s^2)$ . Here we include  $\mathcal{O}(\alpha_s)$  corrections to the coefficients of the  $\mathcal{O}(v^4)$  kinetic terms,  $c_1$ ,  $c_5$  and  $c_6$ , and, for some of the ensembles, the chromomagnetic term,  $c_4$  [16, 23]. The effect of  $\mathcal{O}(\alpha_s)$  corrections to other terms (with coefficients  $c_2$  and  $c_3$ ) at  $\mathcal{O}(v^4)$  will be estimated by looking at the effect of the  $\mathcal{O}(\alpha_s)$  corrections to  $c_4$ . The  $\mathcal{O}(\alpha_s)$  coefficients to  $c_1$ ,  $c_4$ ,  $c_5$  and  $c_6$  are calculated after tadpole-improvement to the gluon field, which means dividing all the links,  $U_\mu(x)$  by a tadpole-parameter,  $u_0$ , before constructing covariant derivatives or  $\mathbf{E}$  and  $\mathbf{B}$  fields for the Hamiltonian above. For  $u_0$  we took the mean trace of the gluon field in Landau gauge,  $u_{0L}$  [16]. Tadpole-improvement means that the  $c_i^{(1)}$  coefficients are typically less than  $\mathcal{O}(1)$ , whereas without tadpole-improvement they can be much larger because of the effect of tadpole diagrams in the lattice theory. The values used for  $U_{0L}$  and  $c_i$  on the different ensembles are given in Table II.

This improved NRQCD action has been used for accurate calculations of the  $\Upsilon$  spectrum [16, 25, 26] and  $B$  and  $B_s$  meson masses [27] and decay constants [24].

Given the NRQCD action above, the heavy quark propagator is readily calculated from its lattice time evolution given by:

$$\begin{aligned}
 G(\mathbf{x}, t+1) &= \left(1 - \frac{a\delta H}{2}\right) \left(1 - \frac{aH_0}{2n_h}\right)^{n_h} U_t^\dagger(x) \tag{2} \\
 &\quad \times \left(1 - \frac{aH_0}{2n_h}\right)^{n_h} \left(1 - \frac{a\delta H}{2}\right) G(\mathbf{x}, t)
 \end{aligned}$$

with starting condition:

$$G(\mathbf{x}, 0) = \phi(\mathbf{x})1. \tag{3}$$

Here 1 is the unit matrix in color and (2-component)

Set	$am_b$	$a\bar{M}_{kin}$	$aE_0$	$u_{0L}$	$c_1, c_6$	$c_5$	$c_4$
1	3.297	7.087(8)	0.27823(5)	0.8195	1.36	1.21	1.0
1	3.297	7.109(10)	0.25137(6)	0.8195	1.36	1.21	1.22
1	3.42	7.303(15)	0.27669(5)	0.8195	1.36	1.21	1.0
2	3.25	6.988(14)	0.24950(2)	0.8195	1.36	1.21	1.22
3	2.66	5.761(14)	0.28458(2)	0.8340	1.31	1.16	1.0
4	2.62	5.717(9)	0.25161(2)	0.8341	1.31	1.16	1.20
5	1.91	4.264(11)	0.27767(2)	0.8525	1.21	1.12	1.0

TABLE II: Summary of the valence  $b$  quark mass and other action parameters for the NRQCD action on the different ensembles of Table I. The  $b$  quark mass in lattice units (column 2) was tuned by calculating the spin-average of the ‘kinetic masses’ of the  $\Upsilon$  and  $\eta_b$  as described in the text and given in column 3. In column 4 we give the corresponding spin-average of the ground-state energies, needed to reinstate the ‘zero of energy’ in the current-current correlator. Results for sets 3 and 5 are from [16]. Column 5 gives the parameter  $u_{0L}$  used for ‘tadpole-improving’ the gluon field [16, 24] and columns 6, 7 and 8 give the coefficients of kinetic and chromomagnetic terms used in the NRQCD action.  $c_1$ ,  $c_5$  and  $c_6$  ( $c_1$  and  $c_6$  have the same value) are correct through  $\mathcal{O}(\alpha_s)$  [16]. For  $c_4$  we used the  $\mathcal{O}(\alpha_s)$  corrected value [16, 23] for sets 2 and 4 but the value 1.0 on sets 1, 3 and 5. The top row of parameters for set 1 are our ‘preferred’ ones and these are the results that will be plotted in Figures, unless stated otherwise. Results for the other values of  $c_4$  (row 2)  $am_b$  (row 3) allow us to judge the effect of changing these parameters.

spin space and  $\phi(\mathbf{x})$  is a simple function of spatial position, often called a ‘smearing function’. We can use such a function because we fix the gluon field configurations to Coulomb gauge. At zero spatial momentum the antiquark propagator is the complex conjugate of the quark propagator for a source of the kind given in eq. (3). The parameter  $n_h$  has no physical significance, but is included for improved numerical stability of high momentum modes that do not contribute to bound states [15]. Here we use  $n_h = 4$  throughout.  $n_h$  also appears in the final term of  $\delta H$  (eq. (1)) because of the correction for the discretisation error in the time derivative [15].

## B. Meson Correlators

Quark and antiquark propagators are combined to form meson correlation functions by matching up color indices and combining appropriate spin indices. We will focus almost entirely on the vector  $\Upsilon$  states here, created at  $\mathbf{x}_1$  with an interpolating operator

$$Y^{(\phi)}(\mathbf{x}_1) = \sum_{\mathbf{x}_2} \psi^\dagger(\mathbf{x}_1) \sigma_i \phi(\mathbf{x}_1 - \mathbf{x}_2) \chi^\dagger(\mathbf{x}_2) \quad (4)$$

where  $\psi^\dagger$  creates a 2-component quark,  $\chi^\dagger$ , an antiquark and  $\sigma_i$  is the Pauli spin matrix  $\sigma_x$ ,  $\sigma_y$  or  $\sigma_z$  for different  $\Upsilon$  polarisations. A meson correlation function that uses this operator at the source ( $sc$ ) and an equivalent operator to destroy the meson at the sink ( $sk$ ) can then be made

by combining quark and antiquark propagators at lattice time  $t$  into

$$\begin{aligned} C(t) &= \langle 0 | [Y_t^{(\phi_{sk})}]^\dagger Y_0^{(\phi_{sc})} | 0 \rangle \\ &= \sum_{\mathbf{y}_1, \mathbf{y}_2} \text{Tr}[\sigma_i G_\delta^\dagger(\mathbf{y}_1, t) \sigma_i \phi_{sk}(\mathbf{y}_1 - \mathbf{y}_2) G_{\phi_{sc}}(\mathbf{y}_2, t)]. \end{aligned} \quad (5)$$

Here  $G_\delta$  is generated using eq. (3) with  $\phi(\mathbf{x})$  set equal to a delta function and  $G_{\phi_{sc}}$  with  $\phi(\mathbf{x}) = \phi_{sc}(\mathbf{x})$ .  $\phi_{sk}$  is the sink smearing function which need not be the same as at the source. The convolution can be implemented using a Fast Fourier Transform. The meson correlation function is projected onto zero spatial momentum by the sum over sink spatial indices and the trace is over color and spin indices.

Meson correlation functions in principle contain all the states of the system consistent with the quantum numbers of the operator used. Here we can restrict ourselves to bottomonium states because we have not allowed any mixing with other sectors; this is expected to have negligible effect for  $\Upsilon$  mesons in any case. By inserting a complete set of states into the first line of eq. (5) we see that the (Euclidean) time dependence of  $C(t)$  is given by:

$$C(t) = \sum_{m=0}^{m_{exp}-1} c(\phi_{sc}, m) c^*(\phi_{sk}, m) e^{-E_m t}. \quad (6)$$

Here  $E_m$  denote the (NRQCD) energies of the ladder of  $m_{exp}$  vector bottomonium states that we include.  $m = 0$  corresponds to the ground-state  $\Upsilon$ ,  $m = 1$  to the  $\Upsilon'$  etc. The components of the amplitude of a given state depend on the overlap of the action of the operator  $Y$  on the vacuum with that state:

$$c(\phi, m) = \langle 0 | Y^{(\phi)} | \Upsilon^{(m)} \rangle / \sqrt{2M_{\Upsilon^{(n)}}}, \quad (7)$$

where  $M$  denotes the meson mass and we use the conventional  $2M$  normalisation for states at rest. From this it is clear that different choices of  $\phi$  allow us to change the contributions of different states to the meson correlator. At large times all correlators are dominated by the ground-state, but at relatively short times meson correlators made with smeared propagators can have very different time-dependence that allows us to extract the properties of excited states.

We used this technique, a standard one in lattice QCD calculations, to determine the masses of the  $\Upsilon'$  and  $\Upsilon''$  in [16]. We used a delta function source and two ‘hydrogen-wavefunction’ smearings, adjusting their radius as we changed the lattice spacing. This enabled us to make a  $5 \times 5$  matrix of meson correlators by combining different smeared quark and antiquark propagators together (i.e. generalising eq. (5) to the case where both propagators have a smeared source). Fitting the elements of this matrix simultaneously to eq. (6) enabled us to extract the energies,  $E_m$ . The differences  $E_1 - E_0$  and  $E_2 - E_0$  correspond to the mass differences between the  $\Upsilon'$  and  $\Upsilon''$  respectively and the  $\Upsilon$ . We determined the lattice spacing in [16] by setting  $E_1 - E_0$  equal to its experimental value.

### C. Tuning Parameters

The ‘zero of energy’ is missing in NRQCD and so to convert mass differences to absolute masses, and hence to tune the quark mass, requires a separate calculation of the energy offset. This is done by calculating the energy of a meson as a function of spatial momentum and determining a ‘kinetic mass’ which can be compared to experiment. This is defined by [12]:

$$aM_{kin} = \frac{\mathbf{p}^2 a^2 - (a\Delta E)^2}{2a\Delta E} \quad (8)$$

for a meson with spatial momentum  $\mathbf{p}$  and with  $\Delta E = E(\mathbf{p}) - E(0)$ . We determine  $E(\mathbf{p})$  and  $E(0)$  for the ground-state  $\Upsilon$  and (pseudoscalar)  $\eta_b$  mesons (i.e.  $m = 0$  in eq. (6)) using only delta function sources for the  $b$  quark propagators. We use a wall of random numbers drawn from  $U(1)$  for these sources, patterned with an appropriate Fourier phase, since this improves statistical accuracy significantly [28]. Although the kinetic mass is independent of the momentum  $\mathbf{p}$  to high accuracy [12] we fix a particular momentum to determine it given by the lattice momentum  $(1, 1, 1)2\pi/L_s$ .

Tuning the  $b$  quark mass means adjusting the value in the action until the kinetic mass for a specific meson agrees with experiment, given a result for the lattice spacing which is used to convert the dimensionless mass  $aM_{kin}$  into physical units. Since our NRQCD action includes only the leading spin-dependent terms (along with their radiative corrections) the kinetic masses for  $\Upsilon$  and  $\eta_b$  show a systematic error in that they appear in the wrong order with the  $\Upsilon$  kinetic mass lower than that of the  $\eta_b$ . As explained in [16] this is because the difference in binding energy from the chromomagnetic term has not been incorporated correctly into the kinetic mass, since a relativistic correction to the chromomagnetic term is required for this to happen. To remove this effect in our quark mass tuning we instead tune the spin-average of the  $\Upsilon$  and  $\eta_b$  masses to experiment, defining

$$\overline{M}_{kin} = \frac{3M_{kin,\Upsilon} + M_{kin,\eta_b}}{4}. \quad (9)$$

The values we obtain at the valence  $b$  quark masses used on each ensemble are given in Table II. The appropriate experimental value to compare this to is the spin-average of experimental  $\Upsilon$  and  $\eta_b$  masses ( $\overline{M}_{\Upsilon,\eta_b}$ ) [29], adjusted for the fact that we are working in a world without electromagnetism (which pushes up both  $\Upsilon$  and  $\eta_b$  masses by an estimated 1.6 MeV [30]). Putting this shift in gives a value for  $\overline{M}_{\Upsilon,\eta_b}$  of 9.446(2) GeV. Here we have taken a 100% error on this shift and also allowed an error (but no shift) for the fact that we do not allow our  $\eta_b$  meson to annihilate to gluons. We earlier estimated the absence of gluon annihilation would shift the  $\eta_b$  mass upwards by approximately 2.4 MeV [30]. Here we simply take this (divided by 4 reflecting the  $\eta_b$  contribution to the spin-average) as an additional uncertainty.

From Table II we see that our  $b$  quark mass is typically tuned at the level of 1%, consistent with the accuracy with which we have determined the lattice spacing. The statistical accuracy on the kinetic mass itself is much better than this. We have used two different quark masses on set 1 so that we can test the  $m_b$  dependence of results. The well-tuned mass on this set is  $am_b = 3.297$  and this is the preferred value for our results.  $am_b = 3.42$  then represents mistuning by 3–4%.

In [16] we discussed the impact of improving the NRQCD action on kinetic masses and properties of the spectrum. For the calculation of this paper we are focussed on the amplitudes given in eq. (7). In Appendix B we show how the  $v^4$  terms in the NRQCD action modify the amplitudes to give improved relativistic covariance.

### D. The Vector Current

Our key result here is for the overlap or matrix element between the vacuum and an  $\Upsilon$  state of an operator  $Y$  which corresponds to the local vector current  $J_V$  that couples to a photon. The hadronic parameter known as the decay constant,  $f$ , is defined for an  $\Upsilon$  at rest, or any of its radial excitations, by

$$\langle 0 | J_{V,i} | \Upsilon_j^{(m)} \rangle = f_{\Upsilon^{(m)}} M_{\Upsilon^{(m)}} \delta_{ij} \quad (10)$$

where  $i$  is the polarisation of the vector current,  $j$  is the polarisation of the  $\Upsilon$  and  $M_{\Upsilon}$  is its mass. The square of the decay constant is then related to the experimentally measurable leptonic width by:

$$\Gamma(\Upsilon^{(m)} \rightarrow e^+ e^-) = \frac{4\pi}{3} \alpha_{QED}^2 e_b^2 \frac{f_{\Upsilon^{(m)}}^2}{M_{\Upsilon^{(m)}}} \quad (11)$$

where  $e_b$  is the  $b$  quark electric charge in units of  $e$  (1/3). The appropriate value for  $\alpha_{QED}$  here is that at the  $b$  quark mass,  $\alpha_{QED}(m_b) = 1/132$  [31]. Higher-order electromagnetic processes are suppressed because the  $\Upsilon$  must decay to an odd number of photons. The experimental values for the leptonic width are accurately known for  $\Upsilon$ ,  $\Upsilon'$  and  $\Upsilon''$  following a dedicated programme by CLEO [32–34].

To determine  $f_{\Upsilon}$  accurately from lattice QCD we need an accurate representation on the lattice, in terms of an operator  $Y$ , of the vector current. Since we are using a nonrelativistic formalism we take a nonrelativistic expansion of the current including leading and next-to-leading order ( $\mathcal{O}(v^2)$ ) corrections. For the vector case the leading operator is given by

$$J_{V,\text{NRQCD},i}^{(0)} = \chi^\dagger \sigma_i \psi. \quad (12)$$

This corresponds to  $Y$  of eq. (4) with the smearing function  $\phi$  set to a delta function. It is therefore one of the standard set of operators that we typically include in the

spectrum calculation. There is only one subleading operator to consider at  $\mathcal{O}(v^2)$  which we can take to be [12, 35]:

$$J_{V,\text{NRQCD},i}^{(1)} = \chi^\dagger \sigma_i \frac{\hat{\Delta}^{(2)}}{(am_b)^2} \psi. \quad (13)$$

$\hat{\Delta}^{(2)}$  is a representation of the  $\Delta^{(2)}$  operator in which we choose (because we are working in Coulomb gauge) not to include the gluon links multiplying the shifted quark fields. This operator is readily implemented at the source by acting with  $\hat{\Delta}^{(2)}$  on a delta function source. At the sink we simply apply  $\hat{\Delta}^{(2)}$  to, say, the quark propagator before combining with the antiquark propagator. There is a further  $\mathcal{O}(v^2)$  operator that has a ‘D-wave’ derivative term [12, 36, 37]. However, since the mixing between the S-wave  $\Upsilon$  states we are considering here and D-wave states is already suppressed by powers of  $v^2$  and observed to be small [25] we can safely neglect that term at this order.

We can then construct a vector current in NRQCD matched order by order in  $v^2$  and  $\alpha_s$  to the continuum vector current whose matrix element appears in eq. (10) and eq. (11). The required matrix element can then be determined in our lattice calculation. At next-to-leading order in  $v^2$  we write

$$\begin{aligned} J_V &= Z_V J_{V,\text{NRQCD}} \\ &\equiv Z_V (J_{V,\text{NRQCD}}^{(0)} + k_1 J_{V,\text{NRQCD}}^{(1)}). \end{aligned} \quad (14)$$

where we have dropped the polarisation index for clarity. From tree-level matching of NRQCD and continuum vector currents  $k_1 = 1/6$ . Calculations in lattice perturbation theory show substantial corrections are possible at  $\mathcal{O}(\alpha_s)$  [35]. Here we determine both  $k_1$  and the overall normalisation,  $Z_V$ , nonperturbatively on the lattice by comparing to continuum QCD perturbation theory for time-moments of the vector current-current correlator. This is described in detail in Appendix A where the values of  $Z_V$  and  $k_1$  obtained are given. Since we use current-current correlator methods both to determine  $Z_V/k_1$  and to determine the  $b$  quark mass, we give here some of the notation and key equations that we use.

## E. Moments

Vector bottomonium correlators  $C_{V,\text{NRQCD}}(t)$  are constructed using  $J_{V,\text{NRQCD}}$  of eq. (14) at source and sink. The time-moments are then defined by:

$$\begin{aligned} G_n^{V,\text{NRQCD}} &= \\ 2 \sum_t (t/a)^n C_{V,\text{NRQCD}}(t) \exp(-[\overline{M}_{kin} - \overline{E}_0]t) \end{aligned} \quad (15)$$

where the factor of 2 is needed to relate the moments to continuum values since the nonrelativistic quark propagators only propagate forwards in time (see eq. (3)) and not in both directions. The moment number  $n =$

$n$	$r_n^{(1)}$	$r_n^{(2)}$	$r_n^{(3)}$
4	0.7623	0.2750	-0.2347
6	0.7727	0.7190	-0.1865
8	0.6102	0.7990	-0.1398
10	0.3500	0.7170	-0.2420
12	0.0248	0.5907	-0.4147
14	-0.3475	0.5018	-0.5806
16	-0.7563	0.5096	-0.6972
18	-1.1935	0.6618	-0.7592
20	-1.6550	0.9958	-0.7894
22	-2.1360	1.5433	-0.8546

TABLE III: Coefficients of the perturbative series  $r_n^V = 1 + \sum_i r_n^{(i)} \alpha_s(\mu)$  for  $\mu = \overline{m}_b(\mu)$ . Results are taken from [38–42] for the case with  $n_l = 4$  light quarks in the sea ( $u, d, s$  and  $c$ ) and no heavy ( $b$ ) quarks ( $n_h = 0$ ), except for  $r_n^{(3)}$ , which uses the  $n_l = 4, n_h = 1$  case from [42].

4, 6, 8, ... The exponential factor gives the NRQCD meson correlator the correct time-dependence by restoring the ‘zero of energy’ missing from the Hamiltonian. We use the values of  $\overline{M}_{kin}$  and the spin-averaged ground-state energy,  $\overline{E}_0$ , obtained from the results of tuning the  $b$  quark mass discussed above and given in Table II.

The NRQCD current-current correlator is related by the  $Z_V$  renormalisation factor for the current to that of the continuum current-current correlator, up to discretisation and relativistic corrections:

$$G_n^V = Z_V^2 G_n^{V,\text{NRQCD}}. \quad (16)$$

Continuum time-moments can be derived [13] from  $q^2$ -derivative moments of the heavy-quark vacuum polarisation function that are calculable in continuum QCD perturbation theory [38–42].

$$G_n^V = \frac{g_n^V(\alpha_s, \mu/m_b)}{[a\overline{m}_b(\mu)]^{n-2}} \quad (17)$$

where  $g_n^V$  is known through  $\mathcal{O}(\alpha_s^3)$  either completely or approximately [42] up to  $n = 22$ . If we work in the  $\overline{MS}$  scheme then  $\overline{m}_b$  is the  $b$  quark mass in that scheme at the scale  $\mu$ . Because the continuum perturbation theory has been obtained to such high order (next-to-next-to-next-to-leading order) we make use of this in our lattice calculation, rather than using lower order lattice QCD perturbation theory.

To reduce discretisation errors and sensitivity to tuning of the lattice  $b$  quark mass we make use of ratios of  $G_n^V$  to the result obtained in the free case, i.e. by setting the gluon field,  $U_\mu(x)$ , to the unit matrix in color space and using tree-level values for all of the coefficients in the NRQCD Hamiltonian. Then

$$G_n^{V,U=1} = 2 \sum_t (t/a)^n C_{V,\text{NRQCD},U=1}(t) \exp(-2m_b t). \quad (18)$$

where now the zero of energy offset is simply twice the  $b$  quark mass in the NRQCD action for that ensemble.

Then

$$R_n^V \equiv G_n^V / G_n^{V,U=1} \quad (19)$$

$$= r_n^V(\alpha_{\overline{MS}}, \mu/m_b) \left[ \frac{m_b}{\overline{m}_b(\mu)} \right]^{n-2}.$$

$r_n^V$  is a perturbative expansion starting with 1, being the ratio of the expansion for  $G_n^V$  to the leading, zeroth order, coefficient and  $m_b/\overline{m}_b$  is the ratio of the lattice NRQCD quark mass and the mass in the  $\overline{MS}$  scheme, i.e. the inverse of the mass renormalisation factor for lattice NRQCD<sup>1</sup>.

Table III gives the perturbative coefficients for the perturbative series for  $r_n^V$  up to and including that for  $\alpha_s^3$  (i.e. next-to-next-to-next-to-leading order). The analytic calculations for the coefficients are done for the vacuum polarisation function of a heavy quark loop with  $n_l$  light quark loops and  $n_h$  quark loops with the same mass as the heavy quark. Since we are working with  $u, d, s$  and  $c$  quarks in the sea but no  $b$  quarks we use, where possible,  $n_l = 4$  and  $n_h = 0$ . However this treats the  $c$  quark mass as zero with potential errors from this of  $\mathcal{O}(\alpha_s^2(m_c/m_b)^2)$ , i.e.  $0.05\alpha_s^2$ . The  $\alpha_s^3$  coefficients are taken from the numerical approximate results in [42] for the case  $n_h = 1$ ,  $n_l = 4$ . From comparing exact formula for the first few moments [38–41], results for different  $n_l$  values and also the double-quark loop results of [43] it is clear that  $n_h$  values differing by 1 make negligible difference at this order. We evaluate the series using  $\alpha_s$  in the  $\overline{MS}$  scheme at the scale  $\mu$  equal to  $\overline{m}_b(\overline{m}_b)$ , thus avoiding additional logarithms of  $\mu/m_b$ . We take  $\alpha_{\overline{MS}}(n_f = 5, M_Z) = 0.1185(6)$  and  $\overline{m}_b(\overline{m}_b) = 4.18(3)$  [29], giving  $\alpha_{\overline{MS}}(n_f = 4, \overline{m}_b(\overline{m}_b)) = 0.2268(24)$ . We take a truncation uncertainty in  $r_n^V$  of  $0.25\alpha_s^3$ , which covers the perturbative error from treating  $m_c$  as zero, the approximations at  $\mathcal{O}(\alpha_s^3)$  and unknown coefficients of size 1 at  $\mathcal{O}(\alpha_s^4)$ . Almost all of the coefficients in Table III for orders below  $\alpha_s^4$  are less than 1.

Here we use  $R_n$  to determine the NRQCD-continuum current matching parameter  $Z_V$  which appears in  $G_n^V$  in eq. (16). For this we need to take ratios of powers of different moments to cancel factors of the quark mass, as described in Appendix A.

### F. The Quark Mass

We also determine the quark mass in the  $\overline{MS}$  scheme from  $R_n$  and for this we need to cancel factors of  $Z_V$ . Since  $Z_V$  appears to the same power in each time-moment the ratio of successive time moments is independent of  $Z_V$ . To extract  $\overline{m}_b$  in terms of a physical quantity we multiply by the ratio of the spin-average of

the  $\Upsilon$  and  $\eta_b$  kinetic masses to twice the lattice NRQCD  $b$  quark mass. Then

$$\left[ \frac{R_n r_{n-2}}{R_{n-2} r_n} \right]^{1/2} \frac{\overline{M}_{kin}}{2m_b} = \frac{\overline{M}_{\Upsilon, \eta_b}}{2\overline{m}_b(\mu)}. \quad (20)$$

for  $n \geq 6$ . From the right-hand side we can determine  $\overline{m}_b$  using the experimental spin-average of the  $\Upsilon$  and  $\eta_b$  masses.

In this way we are able to extract a great deal of physics from the correlator  $C_{V, \text{NRQCD}}(t)$  and the results will be given in Section III.

Having defined the NRQCD current from perturbation theory for the correlator time-moments we can fit  $C_{V, \text{NRQCD}}(t)$  as a function of  $t$  in combination with the matrix of smeared correlators described above and determine the matrix elements of  $J_V$  that give the  $\Upsilon$  and  $\Upsilon'$  decay constants. Hence we can determine their leptonic widths from eq. (11). Simultaneously time-moments of  $C_{V, \text{NRQCD}}(t)$  can be directly compared to inverse  $s$ -moments of the  $b$ -quark contribution to  $\sigma(e^+e^- \rightarrow \text{hadrons})$ . In Section III we give the lattice results for the moments from eq. (15) and compare to the values extracted from experimental results on  $e^+e^- \rightarrow \text{hadrons}$  [44]. A final application is that of the accurate determination of the  $b$  quark mass in the  $\overline{MS}$  scheme using eq. (20).

## III. RESULTS

### A. $\Upsilon$ Leptonic Width

For the leptonic width of the  $\Upsilon$  we need to determine the matrix element given in eq. (7) for the ground state,  $m = 0$ . Since the ground-state dominates the correlation function at large values of  $t$  this can be done from a meson correlation function in which we simply use the local current of eq. (14) at source and sink. By calculating separately the pieces corresponding to  $J_{V, \text{NRQCD}}^{(0)}$  and  $J_{V, \text{NRQCD}}^{(1)}$  we can generate correlation functions for different values of the current correction coefficient  $k_1$  and investigate the effect of that on the determination of the overall renormalisation factor,  $Z_V$ , using continuum perturbation theory for the current-current correlator. This is described in Appendix A and the results we obtain for  $k_1$  and  $Z_V$  are given in Table IX.

We fit the  $2 \times 2$  matrix of correlation functions that correspond to  $J_{V, \text{NRQCD}}^{(0)}$  or  $J_{V, \text{NRQCD}}^{(1)}$  at source and sink to the form given in eq. (6) to extract the ground-state amplitude for each current,  $c(J_{V, \text{NRQCD}}^{(j)}, 0)$ . We use a standard Bayesian fitting approach [45] constraining the amplitudes with priors of width between 3 and 5 times the ground state amplitude, and energy differences between excited states with prior  $600 \pm 300$  MeV. The amplitudes are given, for each set of gluon configurations, in Table IV. Statistical errors are small in this case. Note

<sup>1</sup> Note that, although we follow the same procedure as in [13] our definitions of  $R_n$  and  $r_n$  given here are not the same.

Set	$am_b$	$c_4$	$c(J_V^{(0)}, 0)$	$c(J_V^{(1)}, 0)$	$a^{3/2} f_{\Upsilon} \sqrt{M_{\Upsilon}}$
1	3.297	1.0	0.9422(22)	-0.2439(6)	1.334(4)(33)
1	3.297	1.22	0.9194(24)	-0.2355(7)	1.346(4)(34)
1	3.42	1.0	0.9695(23)	-0.2373(6)	1.376(4)(40)
2	3.25	1.22	0.9087(21)	-0.2371(6)	1.304(3)(35)
3	2.66	1.0	0.7153(17)	-0.2360(6)	0.929(2)(26)
4	2.62	1.20	0.6821(18)	-0.2268(6)	0.914(3)(23)
5	1.91	1.0	0.4523(8)	-0.2109(4)	0.604(1)(11)

TABLE IV: Columns 4 and 5 give the ground-state ( $\Upsilon$ ) amplitudes for operators corresponding to the leading ( $J_V^{(0)}$  abbreviating  $J_{V,\text{NRQCD}}^{(0)}$ ) and next-to-leading ( $J_V^{(1)}$  abbreviating  $J_{V,\text{NRQCD}}^{(1)}$ ) pieces of the NRQCD vector current for  $b\bar{b}$  annihilation (*before* multiplication by  $Z_V$ ). Errors are statistical/fitting errors. Column 6 gives the corresponding values for the decay constant parameter  $f_{\Upsilon} \sqrt{M_{\Upsilon}}$  in lattice units. The first error is statistical and the second from the  $Z_V$  factor used to normalise the current.

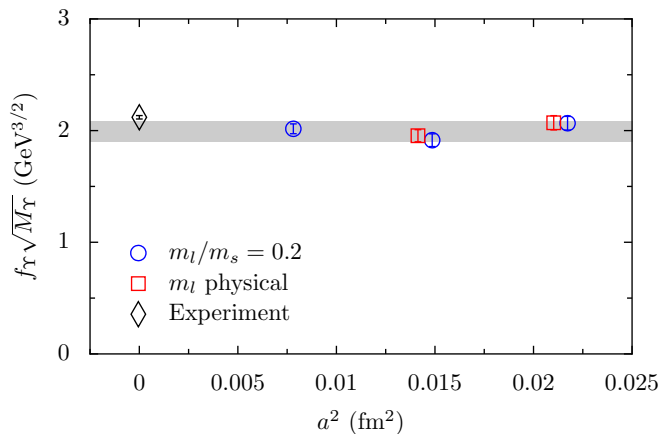


FIG. 1: The hadronic parameter  $f_{\Upsilon} \sqrt{M_{\Upsilon}}$  from our lattice calculation plotted against the square of the lattice spacing. Open blue circles give results from sets 1, 3 and 5 and open red squares, sets 2 and 4. The grey band gives the physical value resulting from a fit to lattice-spacing and sea-quark mass dependence combined with other sources of systematic error as described in the text. The width of the grey band is then twice our total error. The black diamond gives the result derived from the experimental leptonic width using eq. (11).

that the matrix elements of  $J^{(1)}$  are negative, as expected from the form it takes (eq. (13)).

We can combine these amplitudes with the values for  $k_1$  and  $Z_V$  from Table IX to form the amplitude for  $J_{V,i}$ . In fact what we do is to make up correlators that correspond to using operator  $J_{V,i}$  at source and sink and fit that as above to obtain the ground-state amplitude. The two methods give the same result. Multiplying these amplitudes by  $\sqrt{2}$  and  $Z_V$  gives  $f_{\Upsilon} \sqrt{M_{\Upsilon}}$  in lattice units using eqs. (7) and (10). These values are given in the rightmost column in Table IV. The error on the amplitude is dominated by that from  $Z_V$  and, in determining this error, we pay attention to the correlation between the

uncertainty in  $k_1$  and that in  $Z_V$  as given in Table IX <sup>2</sup>.

$f\sqrt{M}$  is the hadronic parameter that is the direct output from our lattice QCD calculation and from which we must determine a physical result to be compared with experiment. The results for  $f\sqrt{M}$  (converted to physical units using the lattice spacing values in Table I) are plotted against the square of the lattice spacing in Figure 1. We see relatively little dependence on either the lattice spacing or the sea quark masses. Table IV also shows that changing the coefficient  $c_4$  in the NRQCD action has insignificant effect. Changing the  $b$  quark mass from 3.297 (well-tuned, and plotted on Figure 1) on set 1 to 3.42 (badly-tuned) has a visible effect and we can use this to estimate tuning uncertainties.

To obtain a physical result from our lattice values we must fit them as a function of lattice spacing and of sea light quark mass. Our results on sets 2 and 4 correspond to a physical value of the  $u/d$  sea mass but in order to incorporate fully any lattice spacing dependence we need also to include sets 1, 3 and 5 in the fit.

For the fits we use the method developed in [16] allowing for both ‘standard’ discretisation errors that come from the gluon or light quark actions but also higher order discretisation errors in the NRQCD action that may have  $am_b$ -dependent coefficients. Adding these terms in to our fit allows them to contribute to the error on the physical result. Since we will use this fit for other quantities we simply denote the hadronic parameter which is the subject of the fit by  $h$ , here  $f_{\Upsilon} \sqrt{M_{\Upsilon}}$ . We use the form:

$$h(a, m_{sea}) = h_{\text{phys}} [1 + b_l \delta m_{sea} / (10m_s) + \sum_{j=1,3} c_j (a\Lambda)^{2j} + \sum_{j=1,2} (a\Lambda)^{2j} [c_{jb} \delta x_m + c_{jbb} (\delta x_m)^2]] \quad (21)$$

The second term in square brackets accounts for the sea quark mass dependence using a simple linear dependence expected at leading order. Since the sea mass dependence is very small this is sufficient.  $\delta m_{sea}$  is the difference between the sum of twice the light and strange sea quark masses and its physical value. The physical values of the  $s$  quark mass (for the lattice spacing values in Table I) are given in [16] and we take the ratio of physical  $s$  to light quark mass as 27.5 [29]. The factor of  $10m_s$  in the denominator is a convenient way (cancelling the mass renormalisation) to introduce the chiral scale of 1 GeV. The third term accounts for standard discretisation errors, using a scale of  $\Lambda$  where we set  $\Lambda = 500$  MeV. The

<sup>2</sup> Note that the normalisation of the amplitudes that we are using here is that appropriate to that of the decay constant. A normalisation that is frequently used instead in NRQCD calculations [12] is that appropriate to determining a wavefunction. The difference between the two normalisations for the amplitude is  $\sqrt{6}$ .

terms containing  $\delta x_m$  allow for discretisation effects with dependence on the  $b$  quark mass in the NRQCD action by modelling this with a linear and quadratic term.  $\delta x_m$  is chosen to vary from -0.5 to 0.5 across our range of masses by taking  $\delta x_m = (am_b - 2.7)/1.5$ . We use eq. (21) within a Bayesian fitting approach [45] taking priors on the coefficients of the fit as 0.0(1.0) except for  $c_1$  which we take as 0.0(0.5) since tree-level  $a^2$  errors are absent from our action and so we expect this term to be at most  $\mathcal{O}(\alpha_s)$ . We take a prior width of 50% on  $h_{\text{phys}}$ .

The physical value for the leptonic width that we obtain from the fit ( $\chi^2 = 0.57$  for 5 degrees of freedom) is 1.995(90) GeV $^{3/2}$ . To this we must add systematic errors corresponding to:

- missing higher order current corrections. These are of  $\mathcal{O}(v^4)$  in a relativistic expansion and so this can be estimated at 1% for the  $\Upsilon$ , where  $v^2 \approx 10\%$ .
- uncertainty in tuning the  $b$  quark mass. This is at most 1% from Table I and II and is mainly a consequence of the uncertainty in the determination of the lattice spacing giving the physical value for  $M_{\text{kin}}$ . From Table IV, comparing results from  $am_b = 3.297$  and 3.42, we see that this leads to a possible 1% uncertainty in the decay constant.
- electromagnetic effects (missing from our calculation). Electromagnetic effects in the  $\Upsilon$  and  $\eta_b$  masses have already been accounted for but at 0.02% are negligible. Effects of the decay constant arising from the additional electromagnetic attraction of quark and antiquark can be estimated from a potential model, to give 0.2% [46].
- missing  $b$  quarks in the sea. The effect of  $b$  quarks in the sea induces a short-distance potential [46] between heavy quarks similar to the hyperfine potential which causes differences between  $f_\Upsilon$  and  $f_{\eta_b}$ . Since these differences are small [47] the effect is negligible.

This gives a final physical result of 1.995(94) GeV $^{3/2}$  with error budget given in Table V. Errors are dominated by those from the lattice spacing dependence and  $Z_V$ . Dividing by the square root of the experimental  $\Upsilon$  mass gives a decay constant result with a 5% uncertainty:

$$f_\Upsilon = 0.649(31)\text{GeV}. \quad (22)$$

In Section IV we will include this value in a summary plot of decay constants from across the meson spectrum.

We can use the experimental value of the  $\Upsilon$  leptonic width, 1.340(18) keV to determine a value of  $f_\Upsilon\sqrt{M_\Upsilon}$  of 2.119(14) GeV $^{3/2}$  (and a value for  $f_\Upsilon$  of 0.689(5) GeV) using eq. (11). The value for  $f_\Upsilon\sqrt{M_\Upsilon}$  is marked on the plot in Figure 1 for comparison to our results. The agreement is good, within  $1.5\sigma$ . The value for  $f_\Upsilon$  will be compared to our results in Figure 6 in the Conclusions. Alternatively we can compute a leptonic width from our

Error	$f_\Upsilon\sqrt{M_\Upsilon}$	$\overline{m}_b(10\text{GeV})$
Statistics	0.3	0.0
$Z_V/k_1$	2.5	0.3
perturbation theory/ $\alpha_s$	-	0.3
uncertainty in $a$	1.6	0.0
lattice spacing dependence	3.4	0.4
sea-quark mass dependence	1.0	0.0
$b$ -quark mass tuning	1.0	0.0
NRQCD systematics	1.0	0.3
electromagnetism $\eta_b$ annihilation	0.0	0.0
total	4.8	0.7

TABLE V: Error budget for the quantities determined in this paper. Errors are given as a percentage of the final answer. For  $f_\Upsilon\sqrt{M_\Upsilon}$  the perturbation theory errors are included in the errors from  $Z_V/k_1$  and not separated. Errors from the lattice spacing dependence are determined from the fit and include NRQCD uncertainties. Errors smaller than 0.1% are denoted by 0.0.

result for  $f_\Upsilon\sqrt{M_\Upsilon}$  using eq. (11), along with the experimental value for the  $\Upsilon$  mass and  $\alpha_{QED}$ . We obtain  $\Gamma(\Upsilon \rightarrow e^+e^-) = 1.19(11)$  keV, again in good agreement with the experimental result.

## B. $\Upsilon'$ Leptonic Width

To determine the  $\Upsilon'$  leptonic width we can make use of the ratio of amplitudes with that of the  $\Upsilon$  to cancel  $Z_V$  and reduce the uncertainty from that source. We also expect lattice spacing and tuning uncertainties to cancel to a large extent. The ratio of the amplitudes for  $J_{V,i}$  in the ground and first-excited states gives:

$$A = \frac{\langle 0|J_{V,i}|\Upsilon^{(1)}\rangle}{\langle 0|J_{V,i}|\Upsilon^{(0)}\rangle} = \frac{f_{\Upsilon'}}{f_\Upsilon} \sqrt{\frac{M_{\Upsilon'}}{M_\Upsilon}}. \quad (23)$$

To determine the properties of excited states accurately it is important to use smeared sources, as described in Section II B and used in [16] to obtain excited state masses. Here we combine results from a local source (corresponding to  $J_{V,\text{NRQCD}}^{(0)}$ ) and sink operator  $J_{V,\text{NRQCD}}^{(1)}$  with the matrix of correlators used in [16]. We use the  $3 \times 3$  matrix of smearings called  $l$ ,  $g$  and  $e$  in [16]. The ‘ $l$ ’ smearing is the local operator corresponding to  $J_{V,\text{NRQCD}}^{(0)}$  so the  $ll$  correlator already has this operator at source and sink. The other correlators in the matrix ( $lg$ ,  $ge$ ,  $gg$  etc [16]) add information about the excited states. From fits to all of the correlators we can then extract matrix elements for  $J_{V,\text{NRQCD}}^{(0)}$  and  $J_{V,\text{NRQCD}}^{(1)}$  in both the ground-state and excited states. We rapidly lose statistical accuracy, however, and so restrict ourselves here to the ground and first excited state. We use 9-exponential fits of the form given in eq. (6) with standard priors on energies and amplitudes ( $600 \pm 300$  MeV on excited state mass splittings and an amplitude prior width corresponding to 3–5 times the ground state local amplitude).



	1	3	5
$am_b$	3.42	2.66	1.91
$c(J^{(0)}, 0)$	0.9720(2)	0.7160(1)	0.4523(1)
$c(J^{(1)}, 0)$	-0.2376(1)	-0.2362(1)	-0.2109(1)
$c(J^{(0)}, 1)$	0.791(8)	0.570(8)	0.360(2)
$c(J^{(1)}, 1)$	-0.277(4)	-0.261(5)	-0.225(1)
$A$	0.854(16)	0.813(14)	0.774(7)

TABLE VI: Amplitudes for the operators corresponding to the leading ( $J_{V,\text{NRQCD}}^{(0)}$ ) (abbreviated to  $J^{(0)}$ ) and next-to-leading ( $J_{V,\text{NRQCD}}^{(1)}$ ) pieces of the NRQCD vector current for both the  $\Upsilon$  (0) and  $\Upsilon'$  (1) mesons.  $A$  is the ratio given in eq. (23). The error on  $A$  includes the error from the uncertainty in  $k_1$ . Results are sets 1 (with  $am_b = 3.42$ ), 3 and 5.

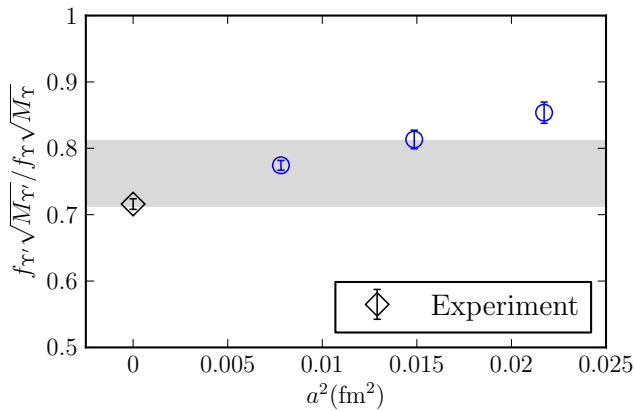


FIG. 2: The ratio of hadronic parameters  $f\sqrt{M}$  for  $\Upsilon'$  to  $\Upsilon$  plotted against the square of the lattice spacing. The grey band gives the physical value resulting from a fit to lattice-spacing combined with other sources of systematic error as described in the text. The width of the grey band is then twice our total error. The black burst gives the result derived from the experimental leptonic widths using eq. (11).

Table VI gives results for the matrix elements for  $\Upsilon$  and  $\Upsilon'$  for sets 1, 3 and 5. The results for the  $\Upsilon$  agree with those from Table IV but are more accurate because of the additional information being used here. For the  $\Upsilon'$  we see that the matrix element for  $J_{V,\text{NRQCD}}^{(0)}$  is smaller in magnitude than that for the  $\Upsilon$  and the matrix element for  $J_{V,\text{NRQCD}}^{(1)}$  is bigger in magnitude. The table also gives the ratio,  $A$ , above, obtained by combining the results using the value of  $k_1$ , along with its uncertainty, obtained in Appendix A. Our set 1 results are for our mistuned (by 4%)  $b$  quark mass but we expect this to make little difference to the ratio.

Figure 2 shows the results for  $A$  plotted against the square of the lattice spacing. We fit the ratio as a function of lattice spacing using the fit form given in eq. (21). We take the same set of priors as those described earlier for the decay constant except that we increase the prior

Set	$am_b$	$c_4$	$n = 4$	$n = 6$	$n = 8$	$n = 10$
1	3.297	1.0	0.0492(6)	0.193(2)	0.307(3)	0.399(4)
1	3.297	1.22	0.0487(6)	0.192(2)	0.306(3)	0.398(4)
1	3.42	1.0	0.0453(6)	0.185(2)	0.299(3)	0.387(4)
2	3.25	1.22	0.0500(7)	0.193(2)	0.306(3)	0.397(4)
3	2.66	1.0	0.0643(8)	0.203(2)	0.308(3)	0.401(4)
4	2.62	1.20	0.0635(7)	0.200(2)	0.302(2)	0.393(3)
5	1.91	1.0	0.0755(9)	0.198(2)	0.297(2)	0.391(3)

TABLE VII: Values for  $(G_n)^{1/(n-2)}$  in  $\text{GeV}^{1/2}$  for  $n = 4, 6, 8$  and  $10$  for each ensemble and set of parameters that we use. Errors are from statistics,  $Z_V$ ,  $k_1$  and the determination of the lattice spacing.

on the conventional  $a^2$  dependence to 1.0 since strong  $a$ -dependence is seen (the fit chooses a slope of 0.8(7) for this term). We allow for light sea quark mass dependence as before, although we might expect these effects to also cancel to a large extent. Our results do not have a lot of information about sea-quark mass dependence since they all come from ensembles with similar light sea quark masses in units of the  $s$  quark mass. This fit parameter then simply contributes 3.5% to the error on the ratio.

The physical value for  $A$  obtained from the fit is 0.762(50), with the uncertainty dominated by the  $a$ -dependence, sea-quark mass dependence and statistics. To this we should add an additional systematic error of 1% for missing  $v^4$  terms in the NRQCD vector current, giving 0.762(51). We do not expect any other sources of systematic error to be significant, for example tuning errors will largely cancel. The experimental value for the ratio of  $f\sqrt{M}$  for  $\Upsilon'$  and  $\Upsilon$  obtained from their masses and decay widths to  $e^+e^-$  via eq. (11) is 0.716(8), marked with a black diamond on Figure 2. Our result is in good agreement with that determined from experiment, but a lot less accurate.

Using the value from Section III A for the decay constant of the  $\Upsilon$  and the experimental ratio of masses, we obtain

$$f_{\Upsilon'} = 0.481(39)\text{GeV}. \quad (24)$$

This will be shown on our summary plot in Section IV, where it can be compared to the experimental result of 0.479(4) GeV determined from the leptonic width.

We can also use our physical value for the ratio  $A$ , the experimental leptonic width for the  $\Upsilon$  and the experimental mass ratio to determine a result for the leptonic width of the  $\Upsilon'$ . We obtain 0.69(9) keV, again in good agreement with the experimental result of 0.612(11) keV [29].

### C. $R_{e^+e^-}$

Given a correctly normalised vector current operator, as described in the previous section and Appendix A, we can return to give values for the time-moments from

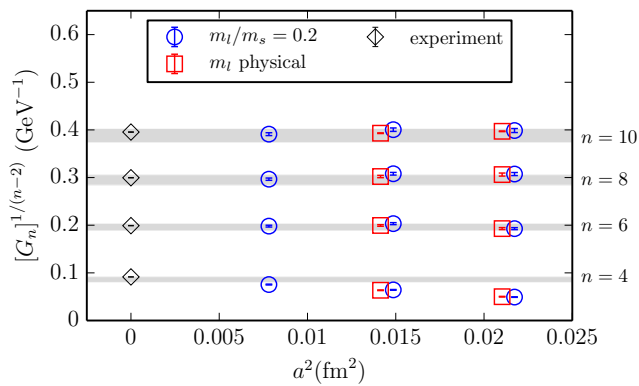


FIG. 3: The  $1/(n-2)$ th root of the  $n$ th time-moment of the vector current-current correlator for (bottom to top)  $n = 4, 6, 8$  and  $10$ , plotted against the square of the lattice spacing. Blue open circles are for sets 1, 3 and 5 and red open squares for 2 and 4. The errors on the points include the uncertainty from  $Z_V$ ,  $k_1$  and the lattice spacing. The grey band shows our physical result with its full error including that from fitting the points and additional systematic errors. The black diamonds are results determined from the experimental data for  $R_{e^+e^-}$

eqs. (15) and (16). Results are given for  $(G_n^V)^{1/(n-2)}$  for  $n = 4$  to  $10$  in Table VII on each of our ensembles. The power  $1/(n-2)$  is taken to reduce all the moments to the same dimension. Figure 3 shows the results plotted against the square of the lattice spacing. The errors on the points come from uncertainty in  $Z_V$  and  $k_1$  (taking account of their correlation) and in the lattice spacing.

We fit the results for each moment as a function of lattice according to the standard fit in eq. (21) using the priors given there, except for the case  $n = 4$  where we increase the width of the prior on the  $a^2$  term to 3.0. Very strong  $a$ -dependence is seen for that case in Figure 3, consistent with the fact that this moment has a big contribution from relatively large spatial momenta.

To the fitted values we must add systematic errors from:

- NRQCD systematics. Our NRQCD vector current is missing relativistic corrections at  $\mathcal{O}(v^4)$ . In Appendix A we estimate that the important spatial momenta for moment  $n$  correspond to  $v^2 \approx 1/n$ . We can test this expectation by studying the effect of the relativistic corrections we include in  $J_{V,\text{NRQCD}}^{(1)}$  (i.e. at  $\mathcal{O}(v^2)$ ). We find shifts for the different moments compared to the leading order result on fine set 5 lattices of  $n = 4$  : 25%,  $n = 6$  : 22%,  $n = 8$  : 18%,  $n = 10$  : 15%. This agrees reasonably well, but is a bit larger, as  $n$  increases, than the naive expectation of  $1/n$ . To determine the systematic error from missing  $v^4$  terms, we therefore take the square of the result we see at  $\mathcal{O}(v^2)$ , giving an uncertainty in the moment of 6% for  $n = 4$ , 4% for  $n = 6$ , 3% for  $n = 8$  and 2% for

$n = 10$ . In the  $1/(n-2)$ th root of the moment, the quantity determined here, the systematic error becomes: 3% for  $n = 4$ , 1% for  $n = 6$ , 0.5% for  $n = 8$  and 0.4% for  $n = 10$ .

- $b$  quark mass tuning. The results in Table VII for set 1 show that mistuning the  $b$  quark mass has a visible effect, with an increasing lattice value for  $am_b$  giving a smaller value for the moment. This is most evident for the 4th moment. Mass tuning relies on the lattice spacing determination and the tuning error arises from the uncertainty in the lattice spacing (since  $\bar{M}_{kin}$  is determined more accurately than  $a$ ). Here the change in the quark mass counteracts the change in lattice spacing so that tuning uncertainties are relatively small. We take 1.5% for the 4th moment and 0.5% for the others.
- electromagnetism. The effect of electromagnetism in experiment (e.g. photons in the final state) missing from our calculation were estimated for the charm case in [8]. The uncertainties were very small there, and will be negligible here because of the smaller electric charge of the  $b$  quark.

Including these systematic uncertainties along with those from the fit above gives the physical results from our calculation:

$$\begin{aligned}
 (G_4^V)^{1/2} &= 0.086(5)(3)\text{GeV}^{-1} \\
 (G_6^V)^{1/4} &= 0.196(8)(2)\text{GeV}^{-1} \\
 (G_8^V)^{1/6} &= 0.295(11)(2)\text{GeV}^{-1} \\
 (G_{10}^V)^{1/8} &= 0.388(15)(2)\text{GeV}^{-1}. \quad (25)
 \end{aligned}$$

The first error is from the fit, taking into account lattice spacing dependence, and the second error is from systematic errors estimated above.

The results agree well with the values extracted for the  $q^2$  derivative moments,  $\mathcal{M}_k$  ( $n = 2k + 2$ ), of the  $b$  quark vacuum polarization using experimental values for  $R_{e^+e^-} = \sigma(e^+e^- \rightarrow \text{hadrons})/\sigma_{pt}$  [48]. These values, appropriately normalised for the comparison to ours, are:

$$\begin{aligned}
 (M_1^{\text{exp}} 4!/(12\pi^2 e_b^2))^{1/2} &= 0.0915(3) \text{ GeV}^{-1} \\
 (M_2^{\text{exp}} 6!/(12\pi^2 e_b^2))^{1/4} &= 0.1991(5) \text{ GeV}^{-1} \\
 (M_3^{\text{exp}} 8!/(12\pi^2 e_b^2))^{1/6} &= 0.2996(5) \text{ GeV}^{-1} \\
 (M_4^{\text{exp}} 10!/(12\pi^2 e_b^2))^{1/8} &= 0.3955(6) \text{ GeV}^{-1}. \quad (26)
 \end{aligned}$$

These are shown as the black diamonds in Figure 3. Our results from lattice NRQCD have significantly larger errors than those derived from experiment. As discussed above this is primarily because of NRQCD systematic errors for these low moments. Nevertheless this provides a good test of QCD that is complementary to our tests using the leptonic width in Sections III A and III B.

One application of our results is to the determination of the effect on the anomalous magnetic moment,

$a_\mu = (g_\mu - 2)/2$ , of the  $\mu$  lepton from coupling to a  $b$  quark loop i.e. that part of the ‘hadronic vacuum polarisation’ (HVP) contribution that comes from  $b$  quarks. We use the method developed in [49] which converts the moments determined above to  $q^2$ -derivatives of the hadronic vacuum polarisation and thereby determines, via Padé approximants, the  $q^2$ -dependence of the integrand required for the contribution to  $a_\mu$ . We obtain  $a_\mu^b = 0.271(37) \times 10^{-10}$  from our lattice results. This can be compared with the result using our approach but substituting the values for the moments extracted from experiment as given in eq. (26) of  $0.307(2) \times 10^{-10}$  or that from using QCD perturbation theory [50] of  $0.29(1) \times 10^{-10}$ .

Our error is sizeable and dominated by NRQCD systematics. This is because the small  $q^2$  region dominates the integral for the contribution to  $a_\mu$  and the integrand there is given almost entirely by the fourth time-moment, which is the one we can determine least well using NRQCD. The  $b$ -quark piece of the HVP contribution to  $a_\mu$  is very small, however, compared to the total hadronic vacuum polarisation contribution which is  $\approx 700 \times 10^{-10}$ . Its error is therefore not critical to the issue of reducing the theoretical uncertainty in the Standard Model result for  $a_\mu$ . It is nevertheless important to have results for this quantity from lattice QCD as a cross-check of other methods. Results using a relativistic formalism for the  $b$  quark should give smaller errors in future for this quantity. See [51] for preliminary results using the HISQ formalism [21] for the  $b$  quarks.

#### D. Mass of the $b$ quark

We can also use our calculation of the time-moments of the vector current-current correlator to determine the mass of the  $b$  quark. The continuum expression for the moments in eq. (17) contains a perturbative series divided by powers of the  $b$ -quark mass in the  $\overline{MS}$  scheme. To obtain the continuum moments from the lattice moments requires multiplication by the current renormalisation factor  $Z_V$  (as in Section III C) and this introduces significant uncertainties in using the moments directly. We can cancel  $Z_V$ , however, in ratios of successive moments (in which the mass does not cancel) and this gives a much more accurate and robust method, because at the same time we can reduce other systematic errors. We also multiply by the ratio of the spin-average of  $\Upsilon$  and  $\eta_b$  kinetic masses to twice the lattice  $b$  quark mass. This cancels factors of the lattice  $b$  quark mass and allows us to extract the  $b$  quark mass in the  $\overline{MS}$  scheme as a ratio to the spin-average of experimental  $\Upsilon$  and  $\eta_b$  masses. The relevant equations are given in eqs. (19) and (20), yielding.

$$\overline{m}_b(\mu) = \frac{\overline{M}_{\Upsilon, \eta_b}}{2} \left[ \frac{R_{n-2} r_n}{R_n r_{n-2}} \right]^{1/2} \frac{2m_b}{\overline{M}_{kin}} \quad (27)$$

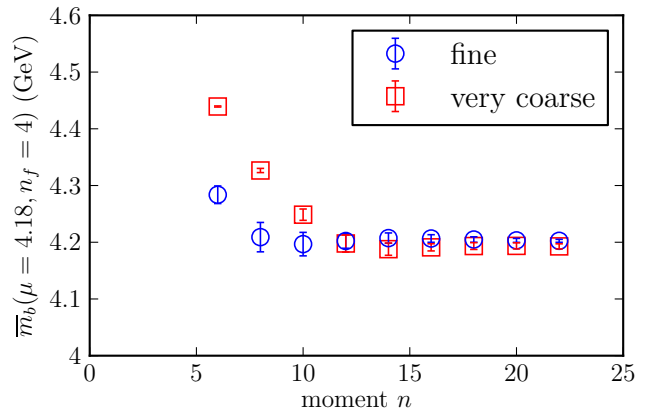


FIG. 4: The  $b$  quark mass in the  $\overline{MS}$  scheme determined from our calculation of time-moments of the vector current-current correlator as a function of the moment number,  $n$ , in eq. (27). Blue open circles are for the fine set 5 lattices and the red open circles for the very coarse set 1. The errors on the points are dominated by the uncertainty in the value of  $k_1$ , the current correction coefficient.

Set	$am_b$	$c_4$	$n = 14$	$n = 18$	$n = 22$
1	3.297	1.0	4.187(11)	4.193(6)	4.192(5)
1	3.297	1.22	4.188(11)	4.194(5)	4.193(6)
1	3.42	1.0	4.189(13)	4.197(6)	4.193(5)
2	3.25	1.22	4.192(11)	4.197(6)	4.196(5)
3	2.66	1.0	4.209(10)	4.210(7)	4.208(4)
4	2.62	1.20	4.210(10)	4.214(7)	4.211(4)
5	1.91	1.0	4.207(9)	4.204(5)	4.202(3)

TABLE VIII: Values for the  $b$  quark mass in GeV in the  $\overline{MS}$  scheme, determined from eq. (27) for  $n = 14, 18$  and  $22$  on each set of configurations that we use. The errors are those from the uncertainty in  $k_1$ ; statistical errors are very small here.

Table VIII gives our results from eq. (27) for  $n = 16, 18$  and  $20$  on all sets and Fig. 4 shows results from sets 1 and 5 as a function of  $n$ . We expect to see  $\overline{m}_b$  reach a plateau as  $n$  increases when internal spatial momenta in the current-current correlator become small enough for our NRQCD vector current to be a good approximation to the continuum vector current and hence to the continuum perturbation theory. In a similar way to that for  $Z_V$  (see Appendix A) we see that this happens down to moment numbers as low as  $n = 8$  in eq. (27) on the fine lattices, but needs somewhat higher moment numbers on the coarser lattices. The results for the two, very different, lattice spacing values agree where they have both reached a plateau.

We consequently take results from  $n = 18$  for our central value and plot these as a function of  $a^2$  in Fig. 5. There is very little dependence on sea-quark mass or lattice spacing. Indeed, as Table VIII also shows, there is very little dependence on the  $c_4$  coefficient in the NRQCD

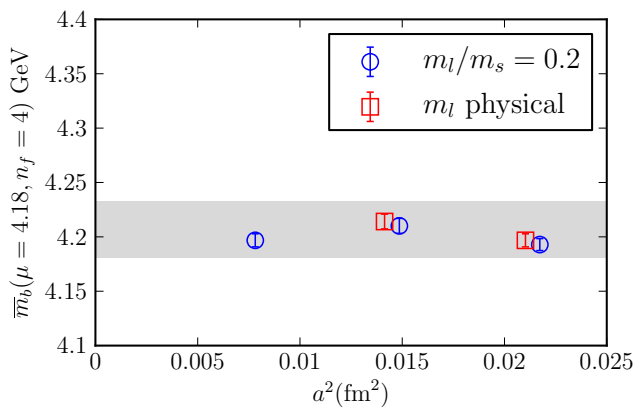


FIG. 5: The  $b$  quark mass in the  $\overline{MS}$  scheme determined from our calculation of time-moments of the vector current-current correlator using eq. (27) with  $n = 18$ . Blue open circles are from sets 1, 3 and 5 and red open squares from sets 2 and 4. The errors on the points include uncorrelated errors only and are dominated by the uncertainty in the value of  $k_1$ , the current correction coefficient. The grey band is the physical value we obtain with its total error, including the error from lattice spacing and quark mass dependence obtained from a fit to the points as well as additional systematic errors described in the text.

action or on the lattice  $b$  quark mass (since this dependence is largely cancelled by  $\overline{M}_{kin}$ ). The errors on the masses are dominated by that from the uncertainty in the value of  $k_1$ ; statistical errors are negligible here. As expected, the error from changing  $k_1$  falls as  $n$  increases and the moments become more nonrelativistic.

To determine a physical value for the mass, we again fit the results as a function of lattice spacing and sea-quark mass, allowing for  $am_b$ -dependent NRQCD errors. We use eq. (21) for the appropriate hadronic parameter, which here is  $\overline{m}_b - \overline{M}_{\Upsilon, \eta_b}/2$ . This is the ‘binding energy’ of the meson which is the consequence of the QCD interactions that we include in our lattice calculation. The physical value for  $\overline{m}_b(\mu = 4.18 \text{ GeV}, n_f = 4)$  that we obtain from our fit is  $4.207(21) \text{ GeV}$ . The result from fitting values from  $n = 14$  or  $22$  are the same within a fraction of  $1\sigma$ . To the error on the physical value we must add systematic errors (which are correlated between the points on Fig. 5 and therefore not included there) from:

- continuum perturbation theory. The perturbative coefficients in our reduced perturbation theory are well-behaved, as shown in Table III. For  $m_b$  we use the square root of the ratio of the perturbative series for successive moments, reducing further the size of the coefficients multiplying powers of  $\alpha_s$  that can appear. We take an error on  $\overline{m}_b$  of  $0.25\alpha_s^3/2$  (the factor of 2 for the square root) which is  $0.15\%$  (7 MeV). This covers uncertainties from missing  $\alpha_s^4$  terms as well as uncertainty in the  $\alpha_s^3$  coefficients [42] and small uncertainties at lower order

from mass effects as discussed in Section II E. A test of this error is simply to miss out the  $\alpha_s^3$  coefficients from our perturbation theory. This increases the value of  $m_b$  we obtain almost uniformly by 5 MeV, so a 7 MeV error on including the  $\alpha_s^3$  coefficients is conservative.

- value of  $\alpha_s$ . Changing the value of  $\alpha_s(m_b)$  by  $1\sigma$  in our perturbative formulae changes the value of  $m_b$  we obtain by 3 MeV (in the opposite direction to the change in  $\alpha_s$ ).
- NRQCD systematics. Our NRQCD action is improved almost completely through  $\alpha_s v^4$ , but we are missing  $v^4$  terms in the vector current. Following Appendix A we estimate the effect of this at  $v^4 \approx (1/n)^2$ . For  $n = 18$  this gives  $0.3\%$  (13 MeV). We can test this estimate by determining masses from using the leading-order current alone (i.e. missing  $v^2$  corrections). We find a shift (downwards) of 30 MeV on very coarse lattices and 8 MeV on fine lattices. So an uncertainty of 13 MeV is conservative for missing higher order  $v^4$  terms in the current.
- $b$  quark mass tuning. This is negligible, as is clear from the entries seen in Table VIII for set 1 at different masses.

Electromagnetic effects appear in the value of the spin-average of  $\Upsilon$  and  $\eta_b$  masses that we use for tuning. This has negligible impact (1 MeV) on the result for  $m_b$ . The effect of missing  $b$  quarks in the sea will be accounted for using perturbation theory below.

Adding the errors above in quadrature gives  $\overline{m}_b(\mu = 4.18 \text{ GeV}, n_f = 4) = 4.207(26) \text{ GeV}$ . To compare results at the conventional point we must convert this to an  $n_f = 5$  quark mass at its own scale and we do this using perturbation theory [52]. We obtain

$$\overline{m}_b(\overline{m}_b, n_f = 5) = 4.196(23) \text{ GeV}, \quad (28)$$

with the error squeezed down by the evolution of the mass to its own scale, but we include an error from uncertainties in this evolution. Evolving to 10 GeV gives a value  $\overline{m}_b(10 \text{ GeV}, n_f = 5) = 3.650(25) \text{ GeV}$ . The error budget for  $m_b$  at the scale 10 GeV is given in Table V.

## IV. CONCLUSIONS

We have presented here the first complete nonperturbative calculation of the leptonic widths of the  $\Upsilon$  and  $\Upsilon'$  using full lattice QCD including  $u, d, s$  and  $c$  quarks in the sea. These are hard calculations to do in lattice QCD because they require an accurate matching of the lattice QCD vector current to the continuum vector current and because they are short-distance quantities, sensitive to discretisation errors. We use a matching method which

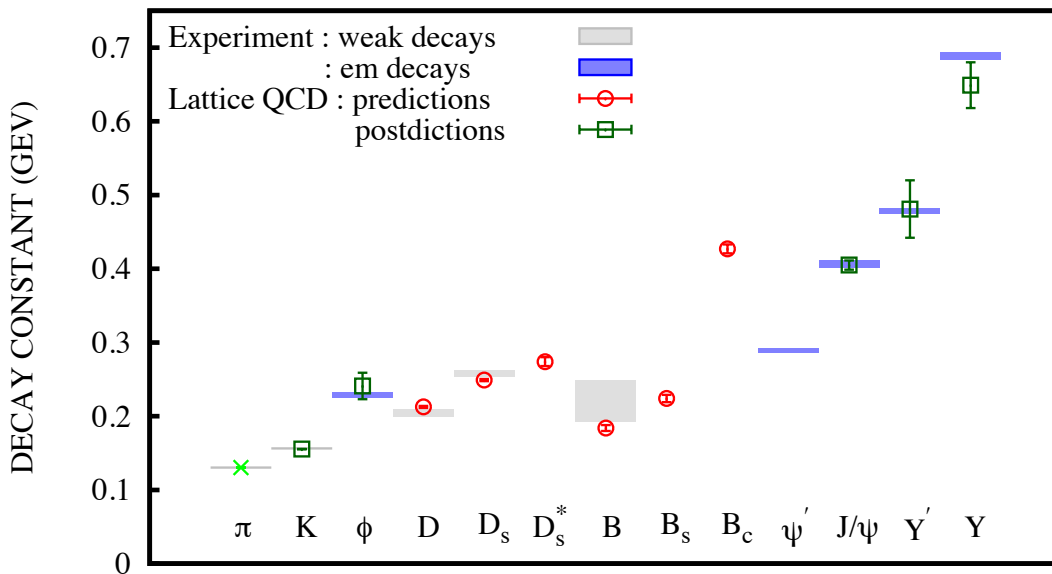


FIG. 6: A summary of values for decay constants of mesons that are narrow and so well-characterised in experiment. The experimental results are taken from appropriate average weak or electromagnetic annihilation rates in the Particle Data Tables [29] and, for weak decays, using average values of the appropriate CKM element. For  $f_K$ ,  $f_D$  and  $f_{D_s}$  experimentally determined values are taken from the decay constant review. For the  $B^+$  we use the average branching fraction [29] obtained by Belle and BaBar [53–56], along with a value for  $V_{ub}$  from a unitarity fit to the CKM matrix [29] to obtain  $f_{B^+} = 0.220(28)$  GeV. For the lattice QCD results we use world’s best values. They are divided into predictions, in which lattice calculations originally predated an experimental result, and postdictions, in which good experimental values existed before lattice results. The lattice result for  $f_\pi^+$  is marked with a cross to indicate that it has been used to set the scale for some analyses (although not here).  $\phi$ ,  $J/\psi$ ,  $D_s^*$ ,  $\eta_c$ ,  $\eta_b$  and  $B_c$  results come from [8, 46, 47, 57, 58] using  $n_f = 3$  configurations. For  $K^+$  we use our results on the  $n_f = 4$  configurations used here [59] and for  $D$  and  $D_s$  we use recent results from the MILC/Fermilab Lattice collaborations on these configurations [60], updating our earlier results on  $n_f = 3$  configurations [46, 61]. For  $B$  and  $B_s$  we use our results on the  $n_f = 4$  configurations using NRQCD  $b$  quarks as here [24]. Finally, the decay constants for  $\Upsilon$  and  $\Upsilon'$  come from this paper.

is nonperturbative on the lattice, making use of high-order continuum QCD perturbation theory. We obtain 5% uncertainty on the  $\Upsilon$  decay constant and 8% on that of the  $\Upsilon'$  (7% uncertainty on the ratio of the two).

Our results are:

$$\begin{aligned} f_\Upsilon &= 0.649(31) \text{ GeV} \\ f_{\Upsilon'} &= 0.481(39) \text{ GeV} \end{aligned} \quad (29)$$

giving leptonic decay widths:

$$\begin{aligned} \Gamma(\Upsilon \rightarrow e^+e^-) &= 1.19(11) \text{ keV} \\ \Gamma(\Upsilon' \rightarrow e^+e^-) &= 0.69(9) \text{ keV} \end{aligned} \quad (30)$$

in good agreement with experiment.

In Figure 6 we summarise lattice QCD results for decay constants of well-characterised mesons with comparison to experimental results determined from weak (for charged pseudoscalars) or electromagnetic (for neutral vectors) decays. This is an update of the summary given in [47]. To determine decay constants from experimental results for weak decays we use average values for the appropriate Cabibbo-Kobayashi-Maskawa (CKM)

matrix elements from the Particle Data Tables [29]. The lattice results given in the Figure all come from simulations that include  $u, d, s$  quarks in the sea or (as here)  $u, d, s$  and  $c$  quarks in the sea. The figure demonstrates the ability of lattice QCD to cover a wide range of physics results working simply with the QCD Lagrangian and the input parameters for QCD. The agreement with experiment is good (within  $2\sigma$ ), where experimental results are available. Lattice QCD is also able to make predictions (given by violet circles in the Figure - some of these now also have experimental results) and confidence in the reliability of these is enhanced by the fact that they sit within this wider picture.

The results for  $\Upsilon$  and  $\Upsilon'$  from this paper are in fact the least accurate. To improve these results in future requires further study of the current correction operators in the nonrelativistic expansion of the vector current. Different representations of this current will have different matrix elements and different ‘mixing-down’ behaviour with the leading-order current which may reduce uncertainties in  $Z_V$  and discretisation effects. Higher-order current corrections should also be considered. Finer lattices, with a spacing of  $a \approx 0.06$  fm are also available [20] and calcula-



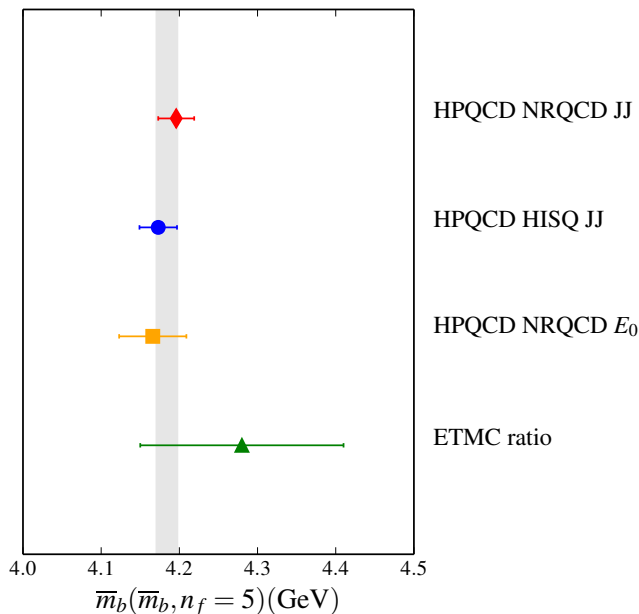


FIG. 7: Lattice QCD results for  $m_b$  in the  $\overline{MS}$  scheme with 5 flavours and evaluated at its own scale. Results are from calculations that include either 3 or 4 flavours of sea quarks and so can be perturbatively corrected to 5 flavours. All 4 results use different methods, indicated on the right. The top result is from this paper, the second from [62], the third from [17] and the fourth from [63], adjusted perturbatively to  $n_f = 5$ . The grey band gives the weighted average of the lattice results: 4.184(15) GeV.

tions on these would have reduced discretisation errors, for example in the ratio of  $\Upsilon'$  to  $\Upsilon$  decay constants.

Since our method uses time-moments of the vector heavyonium correlation function we are also able to compare results directly to values for low moment number derived from experiment for  $\sigma(e^+e^- \rightarrow \text{hadrons})$  in the  $b$  quark region. We find good agreement, although NRQCD systematic errors are large for these moments. Improved results will come from the use of relativistic formalisms such as HISQ. Our results can be converted into the first lattice result for the  $b$  quark contribution to the anomalous magnetic moment of the muon,  $a_\mu^b = 0.271(37) \times 10^{-10}$ .

Finally we give a new determination of the  $b$  quark mass from matching ratios of time-moments of the vector current-current correlator to continuum QCD perturbation theory through NNNLO. Our result is

$$\overline{m}_b(\overline{m}_b, n_f = 5) = 4.196(23) \text{ GeV} \quad (31)$$

with an error that puts this result among the best lattice QCD determinations of this Standard Model parameter.

Figure 7 gives a summary plot of lattice QCD results for  $m_b$ . We compare values obtained on configurations that include either  $u, d, s$  or  $u, d, s, c$  quarks in the sea and can then be converted into a value for  $\overline{m}_b(\overline{m}_b, n_f = 5)$

by adding in the  $c, b$  or  $b$  quarks respectively using perturbation theory. The four results use different methods. The top result is from the work described here. The second [62] uses the relativistic HISQ formalism for the  $b$  quark and pseudoscalar current-current correlators that are absolutely normalised on the lattice. Low moments ( $n = 4 - 10$ ) are compared to continuum QCD perturbation theory for a range of masses up to the  $b$  quark mass on the finest lattices. Results are combined from  $n_f = 3$  and  $n_f = 4$  calculations, updating [14]. The third [17] calculates the quark mass from the binding energy for  $\Upsilon$  and  $B_s$  mesons using the NRQCD formalism on  $n_f = 3$  gluon field configurations. This combines the nonperturbative lattice calculation with continuum QCD perturbation theory for the mass renormalisation and lattice QCD perturbation theory for the heavy quark self-energy, both through  $\mathcal{O}(\alpha_s^2)$ , in a method developed in [64]. The fourth result uses the twisted mass formalism for a range of quark masses from  $c$  to  $b$  on configurations that include  $n_f = 4$  sea quarks. A ratio is taken of heavy-light meson masses to quark masses, for successively larger masses in a procedure that has a well-defined static (infinite quark mass) limit. This allows interpolation to the  $b$  quark mass. The result given of 4.29(13) GeV is for  $n_f = 4$ . Perturbative adjustment to  $n_f = 5$  gives 4.28(13) GeV and that is the value plotted in Figure 7.

The results all have very different systematic errors. Even the two results that use current-current correlator methods are working in a very different range of moment number requiring different methods (i.e. a direct extraction vs using a ratio of moments) with different mesons and a different quark action. There is therefore no obvious correlation between the results and we can take a weighted average to obtain 4.184(15) GeV, plotted as the grey band in Figure 7. This result is very compatible with, but twice as accurate as, the current evaluation in the Particle Data Tables [29]. The value also agrees well with determinations from continuum methods, for example using  $R_{e^+e^-}$  results in the  $b$  region [48].

The method we have given here is applicable to other lattice formalisms for heavy quarks, for example that of the Fermilab Lattice Collaboration [65]. Further determinations of  $m_b$  from other formalisms would be useful in the long-term goal of reducing uncertainties in Standard Model parameters needed for precision characterisation of the Higgs boson.

**Acknowledgements** We are grateful to the MILC collaboration for the use of their configurations and to R. Horgan for useful discussions. Computing was done on the Darwin supercomputer at the University of Cambridge as part of STFC's DiRAC facility. We are grateful to the Darwin support staff for assistance. Funding for this work came from STFC, the Royal Society, the Wolfson Foundation and NSF.

## Appendix A: Determination of $Z_V$

The perturbative analysis of heavy-heavy current-current correlators is well developed in continuum QCD perturbation theory [38–42] and here we make use of that to normalise the lattice NRQCD vector current for  $b\bar{b}$  annihilation that we use to determine the  $\Upsilon$  leptonic width. The method is a variation of that used for the  $J/\psi$  leptonic width in [8]. In that case we were working with a relativistic discretisation of the QCD quark action on the lattice. Since here we have a nonrelativistic discretisation there are some differences in the approach that we lay out in this section<sup>3</sup>.

Time-moments of current-current correlators, being ultraviolet-finite quantities, can be calculated in lattice QCD and extrapolated to the continuum limit to give a continuum result that can be compared to experiment [8]. The current used in the correlator must be matched to the continuum current, however. When the Highly Improved Staggered Quark discretisation [21] is used, for example, the local pseudoscalar density is absolutely normalised [13, 14] but the vector current normalisation has to be fixed. For heavy quarks this can be done using the continuum QCD perturbation theory for the vector current-current correlator moments. The multiplicative renormalisation factor  $Z_V$  is simply determined by matching the lattice result at a given lattice spacing for a specific moment to the perturbative result. We can choose which moment to use, since differences in  $Z_V$  that arise from a different choice are discretisation effects that must disappear in the continuum limit, along with other discretisation errors that result from working at a non-zero lattice spacing. The low moments, 4–10, are known through  $\mathcal{O}(\alpha_s^3)$  so are clearly to be preferred over higher ones. It is convenient to use ratios of vector to pseudoscalar current-current correlator moments since then factors of the quark mass cancel [8].

When a nonrelativistic discretisation of the QCD quark action is used, neither the pseudoscalar nor the vector currents is absolutely normalised and the lattice current is only determined to a given order in a relativistic expansion. Hence the match to continuum QCD perturbation theory has both discretisation errors and relativistic errors, which are mixed by the higher dimension operators used to implement corrections, and so we cannot simply take a value of  $Z$  from the match for a specific moment.

In determining the normalisation of the current we can, however, make use of the fact that time-moments with low moment number emphasise very short times in the current-current correlator and are therefore sensitive to much higher internal spatial momenta within the quark-antiquark pair (the overall momentum of the

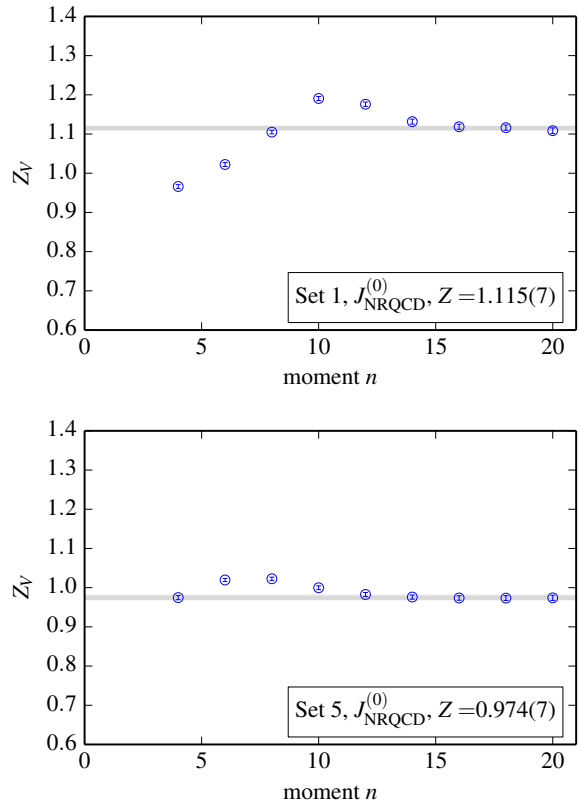


FIG. 8: Renormalisation factor  $Z_V$  for the leading term in the NRQCD vector current,  $J_{V,i,\text{NRQCD}}^{(0)}$ , determined from continuum QCD perturbation theory for the current-current correlator using eq. (A8) and plotted as a function of moment number,  $n$ . The top plot shows results on the very coarse lattices, set 1 (for  $am_b = 3.297$ , the preferred value), and the lower plot shows results on the fine lattices, set 5. The error on the points includes uncertainty in the continuum perturbation theory. The grey bands give the results of a fit to a constant for range 16–20 for set 1 and 14–20 for set 5.

pair is zero) than higher moments are [14]. Thus, as the moment number changes, the sensitivity to relativistic corrections changes. This is easily seen in an analysis of the free case. At leading relativistic order, for vector or pseudoscalar moments, multiplying the free quark and antiquark propagators together we have

$$G_n = 4 \int d^4x t^n \int \frac{dE_1 d^3p_1}{(2\pi)^4} \frac{dE_2 d^3p_2}{(2\pi)^4} \frac{e^{-2mt} e^{i(E_1+E_2)t} e^{i(\mathbf{p}_1+\mathbf{p}_2)\cdot\mathbf{x}}}{(iE_1 + p_1^2/2m)(iE_2 + p_2^2/2m)} \quad (\text{A1})$$

where the quarks have mass  $m$ . Integrating over  $\mathbf{x}$  and  $\mathbf{p}$  gives

$$G_n = 4 \int dt t^n \Theta(t) e^{-2mt} \int \frac{d^3p}{(2\pi)^3} e^{(-p^2/m)t}. \quad (\text{A2})$$

Performing the integral over  $t$  allows us to study the contribution to the integral as a function of  $v^2$ , the square

<sup>3</sup> Note also that, in a nonrelativistic formalism, the annihilation and scattering currents do not have the same renormalisation factor

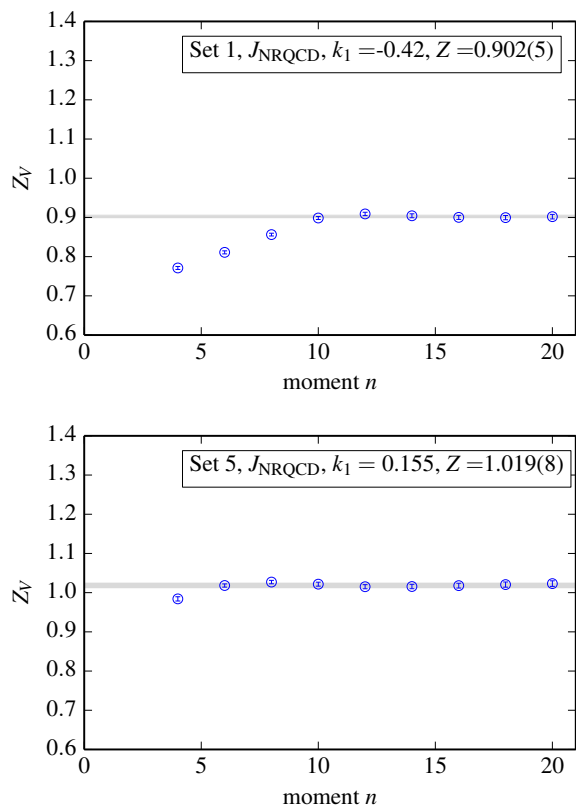


FIG. 9: Renormalisation factor  $Z_V$  for the NRQCD vector current including leading and next-to-leading terms,  $J_{V,i,\text{NRQCD}}^{(0)} + k_1 J_{V,i,\text{NRQCD}}^{(1)}$ , plotted as a function of moment number,  $n$ . From top to bottom results are from very coarse set 1 and fine set 5. The error on the points includes uncertainty in the continuum perturbation theory. The grey bands give the results of a fit to a constant in each case.

of the heavy quark velocity (in units of  $c^2$ ) in the quark-antiquark pair and the expansion parameter in the non-relativistic expansion. In

$$G_n = \frac{n!}{\pi^2 2^{n+1} m^{n-2}} \int \frac{(v^2)^{1/2} d(v^2)}{(1 + v^2/2)^{n+1}} \quad (\text{A3})$$

the integrand peaks at  $v^2 = 1/(n + 1/2)$ , falling as expected with increasing  $n$ .

We therefore expect that the comparison of continuum QCD perturbation theory to the NRQCD correlator moments will in general be poor at very small moment number ( $n = 4, \dots$ ), where the internal velocity within the quark-antiquark pair can be large and NRQCD, as an expansion in  $v^2$ , will have sizeable systematic errors. The comparison will improve as the moment number increases ( $n \geq 6$ ) and the internal momentum falls to non-relativistic values. The improvement will be visible as the development of a plateau region in a plot of the renormalisation constant  $Z_V$  as a function of moment number. This will happen at a moment number where discretisation and relativistic corrections missing from the NRQCD

calculation have become small compared to the unknown higher order terms in  $\alpha_s$  in the continuum perturbation theory expansion for  $Z_V$ .

As discussed in Section IID we calculate NRQCD vector current-current correlators using a local NRQCD current at source and sink,  $J_{V,\text{NRQCD}}$ . Allowing for a renormalisation of this current to match the continuum vector current we have

$$J_{V,i} = Z_V J_{V,\text{NRQCD},i}. \quad (\text{A4})$$

Time moments of the vector correlator calculated from  $J_{V,\text{NRQCD}}$ ,  $C_{V,\text{NRQCD}}(t)$ , are then related to those from the continuum current,  $G_n^V$ , by

$$\begin{aligned} G_n^V &\equiv Z_V^2 C_n^V \\ &= 2Z_V^2 \sum_t (t/a)^n C_{V,\text{NRQCD}}(t) \exp(-[\overline{M}_{kin} - \overline{E}_0]t) \end{aligned} \quad (\text{A5})$$

up to discretisation and relativistic correction terms, where we reproduce eq. (15) from Section IIE.  $G_n^V$  is given by a perturbative expansion

$$G_n^V = \frac{g_n^V(\alpha_s, \mu/m_b)}{(a\overline{m}_b(\mu))^{n-2}} \quad (\text{A6})$$

where  $g_n^V$  is known through  $\mathcal{O}(\alpha_s^3)$  [38–42].  $\overline{m}_b$  is the  $b$  quark mass in the  $\overline{MS}$  scheme.

Dividing by the tree-level value for the correlator moments reduces both relativistic and discretisation errors.  $Z_V$  is then given by

$$Z_V^2 = \frac{C_n^{V,U=1}}{C_n^V} r_n^V \left( \frac{m_b}{\overline{m}_b} \right)^{n-2} \quad (\text{A7})$$

where  $C_n^{V,U=1}$  is the appropriate time-moment of the free NRQCD correlator (with the coefficients in the NRQCD action of eq. (1) set to their tree-level values of 1),  $m_b$  is the quark mass in the NRQCD Hamiltonian and  $r_n^V$  is the perturbative series  $g_n^V$  divided by its leading,  $\mathcal{O}(\alpha_s^0)$  result and for which coefficients are given in Table III. Taking appropriate powers to cancel factors of the quark mass means that we can extract  $Z_V$  from a ratio using different moments:

$$Z_V = X_n^{(n'-2)/(2(n'-n))} / X_{n'}^{(n-2)/(2(n'-n))} \quad (\text{A8})$$

with

$$X_n = \frac{C_n^{V,U=1}}{C_n^V} r_n^V. \quad (\text{A9})$$

We will simply use  $n' = n + 2$ . We evaluate  $r_n^V$  using  $\mu = m_b$  and take  $\alpha_{\overline{MS}}(n_f = 4, m_b) = 0.2268(24)$  [29].

Figure 8 shows an example of this approach in the case where the NRQCD current operator used is the leading term in the relativistic expansion of the current,  $J_{V,\text{NRQCD},i}^{(0)} \equiv \chi^\dagger \sigma_i \psi$  (eq. (12)). We see a plateau in  $Z_V$  for moments between 14 and 20 for very coarse lattices and 12 to 20 for fine lattices. The errors on the points



Set	$am_b$	$c_4$	$k_1$	$Z_V$
1	3.297	1.0	-0.42(16)	0.902(5)(58)
1	3.297	1.22	-0.29(15)	0.963(5)(60)
1	3.42	1.0	-0.52(20)	0.890(5)(67)
2	3.25	1.22	-0.36(16)	0.926(5)(62)
3	2.66	1.0	-0.18(10)	0.865(6)(59)
4	2.62	1.20	-0.11(9)	0.913(6)(50)
5	1.91	1.0	0.155(35)	1.019(8)(35)

TABLE IX: Values for  $k_1$  and  $Z_V$  of eq. (A10) obtained from our current matching procedure for the NRQCD vector current (see text for details). Two errors are given for  $Z_V$ . The first is from the fit for  $Z_V$  at the central value of  $k_1$  and is dominated by that from truncation errors in the continuum perturbation theory and statistical errors in the determination of the meson kinetic mass. The second comes from the uncertainty in  $k_1$  and is correlated with that uncertainty, so that  $Z_V$  increases as  $k_1$  increases.

include the truncation errors from the continuum perturbation theory, taken as  $0.25\alpha_s^3$  to include uncertainty at this order [42], unknown terms at higher orders and possible missing mass-effects at lower orders. The statistical errors from the calculation of the NRQCD correlators are very small but the statistical error in the determination of the kinetic mass that appears in the time-moments (eq. (15) is significant here. Nonperturbative contributions to the moments from the gluon condensate divided by the fourth power of the quark mass, discussed at length for charmonium correlators in [13, 14, 62], are negligible here because of the size of the  $b$  quark mass.

The  $Z$  values given in Figure 8 are obtained from fitting the results to a constant over the range of moment number. We use 14–20 on the fine lattices ( $\chi^2/\text{dof} = 0.05$ ) and 16–20 on the very coarse ( $\chi^2/\text{dof} = 0.6$ ).

Our NRQCD Hamiltonian is completely improved through  $\mathcal{O}(v^4)$  (eq. (1)), which is next-to-leading order in the relativistic expansion. We also include almost all corrections at  $\mathcal{O}(\alpha_s v^4)$ . We therefore expect that the behaviour of  $Z_V$  for moment numbers at the low end of the plateau in Figure 8 can be improved by the addition of next-to-leading order relativistic corrections to the current, since the current  $J_{V,\text{NRQCD}}^{(0)}$  is the only source of errors at this order. In fact we can use this to determine the coefficient of the current correction term nonperturbatively.

We take, as in eq. (14),

$$J_{V,i} = Z_V(J_{V,\text{NRQCD},i}^{(0)} + k_1 J_{V,\text{NRQCD},i}^{(1)}) \quad (\text{A10})$$

and use the behaviour of  $Z_V$  to determine  $k_1$ . Since there is only one relativistic (and discretisation) current correction operator at this order, this is straightforward to do.

Figure 9 shows the behaviour of  $Z_V$  for our preferred values of  $k_1$  on the very coarse and fine lattices. Note that the  $C_n^{V,U=1}$  needed for the ratio in eq. (A9) is calculated with the tree-level value of  $k_1$  i.e.  $1/6$ . By adjusting  $k_1$  we are able to achieve a plateau in  $Z_V$  down to  $n = 10$  or below in all cases. To achieve a plateau in  $Z$  to lower  $n$

values would require current corrections at higher order in  $v^2$  (and  $a^2$ ). We take the central value of  $k_1$  as the point of minimum  $\chi^2/\text{dof}$  (0.8 for set 1, 0.2 for set 3 and 0.4 for set 5) and the uncertainty on  $k_1$  as the range that gives  $\Delta\chi^2/\text{dof} = 1$ .

The corresponding values of  $k_1$  and  $Z_V$  obtained are given in Table IX. The  $k_1$  values agree well with those from matching the NRQCD vector current using  $\mathcal{O}(\alpha_s)$  lattice QCD perturbation theory [35] (although note that this perturbation theory is not directly applicable to our calculation). There it was found that, at a quark mass value  $am_b$  close to that we use on the fine lattices, the  $\mathcal{O}(\alpha_s)$  corrections to  $k_1$  were very small, leaving it at its tree-level value of  $1/6$ . At larger values of  $am_b$ , corresponding to our coarser lattices, the  $\mathcal{O}(\alpha_s)$  corrections to  $k_1$  became large and negative, dominating the tree-level result and leading to a change in sign for  $k_1$ .

The value for  $Z_V$  depends on  $k_1$  because radiative corrections to the current corrections can generate the leading-order current in a process known as ‘mixing down’ [35]. Thus the  $Z_V$  values given in Table IX have two errors. The first comes from the fit result at a fixed value of  $k_1$  and the second comes from the uncertainty in  $k_1$  and is correlated with that uncertainty. The uncertainty in  $k_1$  is estimated as described above and is sizeable. However the associated shift in  $Z_V$  has the effect of counteracting this change when determining the decay constant (as expected for a mixing-down effect) so that the uncertainty in that quantity is significantly smaller than the errors in Table IX naively imply (see Section III A). We also see, from that Table that, as expected for a renormalisation constant, the values for  $k_1$  and  $Z_V$  do not change significantly between sets at approximately the same value of the lattice spacing.

The NRQCD current that we obtain with the values of  $k_1$  and  $Z_V$  given here still has systematic errors from missing current corrections at  $\mathcal{O}(v^4)$ . These errors will be accounted for in the error budget for the different quantities that we determine using this current in Section III.

## Appendix B: Tests of relativistic covariance of NRQCD correlators

As part of testing the NRQCD framework, it is important to check for consistency against relativistic behaviour as NRQCD is improved. Here we provide tests of amplitudes that complement earlier results [16] on meson energies. The tests involve studies of the amplitudes of the leading order NRQCD vector current ( $J_{V,\text{NRQCD}}^{(0)}$ ) for mesons of non-zero spatial momentum. Since the rest of this paper looks at an improved NRQCD current and mesons with zero spatial momentum, the results here are not directly relevant to the rest of our results. They are nevertheless useful as part of the NRQCD ‘bigger picture’ and so we include them here as an Appendix.

As relativistic corrections are added to the NRQCD action it starts to behave, not surprisingly, more like a

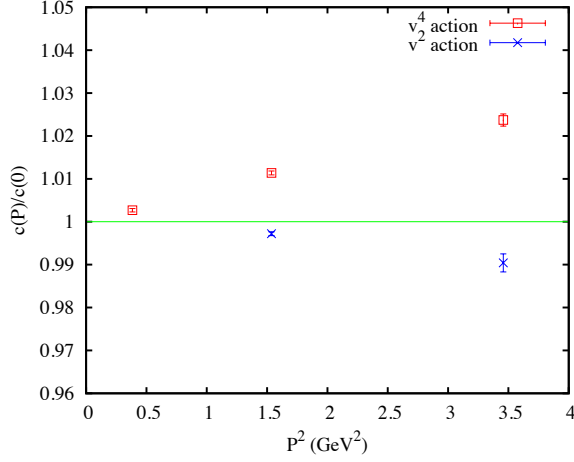


FIG. 10:  $\eta_b$  correlator amplitudes as a function of the square of the  $\eta_b$  spatial momentum. Amplitudes are given as a ratio to the zero momentum amplitude. Results are from set 5 fine configurations. Blue crosses indicated results from a purely  $v^2$  NRQCD action ( $H_0$  only) and red squares give results from the full  $v^4$  action used here (eq. (1)).

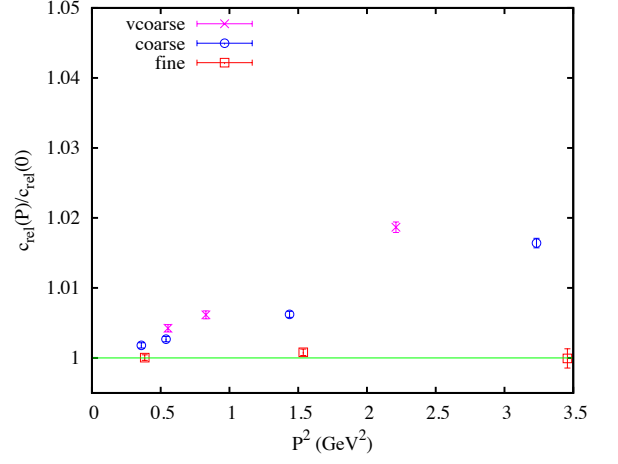


FIG. 12: Pseudoscalar current matrix elements derived from NRQCD  $\eta_b$  correlator amplitudes by applying the matching factor given in eq. B5 as a function of the square of the  $\eta_b$  spatial momentum. Amplitudes are given as a ratio to the zero momentum amplitude. Results are from very coarse set 1 (pink crosses), coarse set 3 (blue circles) and fine set 5 (red squares). The green line shows  $P$ -independent behaviour.

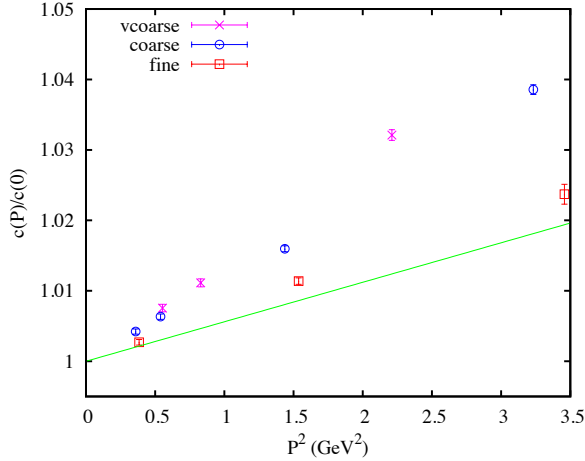


FIG. 11: Temporal axial current matrix elements derived from NRQCD  $\eta_b$  correlator amplitudes as a function of the square of the  $\eta_b$  spatial momentum. Amplitudes are given as a ratio to the zero momentum amplitude. Results are from very coarse set 1 (pink crosses), coarse set 3 (blue circles) and fine set 5 (red squares). The green line gives the ratio of meson energy to mass, using the experimental value for the  $\eta_b$  mass.

relativistic action. In [16] (see also [66]) the behaviour of the meson energy as a function of spatial momentum was discussed, in particular the rôle of  $v^4$  corrections to the action in feeding the meson binding energy into the kinetic mass of eq. (8), so that the dispersion relation for energy as a function of momentum is correct.

Here we discuss the behaviour of the ground-state amplitudes/overlaps for mesons made from quark propaga-

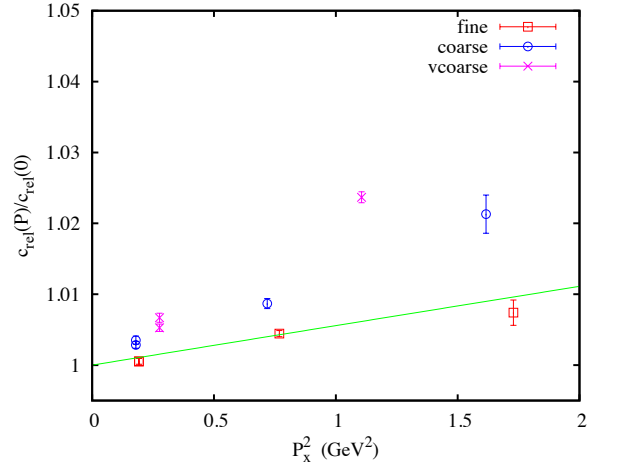


FIG. 13: Vector current matrix elements derived from NRQCD  $\Upsilon$  correlator amplitudes for the case of a current with polarisation  $x$  at both source and sink and meson momentum  $\mathbf{P}$  of the form  $(p, p, 0)$  or  $(p, p, p)$ .  $c_{rel}$  is obtained from  $c$  by applying the matching factor given in eq. B6. Amplitudes are given as a ratio to the zero momentum amplitude. Results are from very coarse set 1 (pink crosses), coarse set 3 (blue circles) and fine set 5 (red squares). The green line shows the expected behaviour as  $\sqrt{1 + P_x^2/M_\Upsilon^2}$ , using the experimental value of the  $\Upsilon$  mass. On all 3 lattices the leftmost points correspond to momentum (in units of  $2\pi/L_s$ ) of  $(1,1,0)$  and  $(1,1,1)$ . On the fine lattices these two points are on top of each other.

tors from a delta function source,  $\phi(x) = \delta(x)$  in eq. (3). This corresponds to the leading order vector current,  $J_{V,\text{NRQCD}}^{(0)}$  (eq. (12)), in the case of vector mesons and the leading order current  $J = \chi^\dagger \psi$  for pseudoscalar mesons. We study the amplitudes for these operators (eq. (6)), as a function of spatial momentum and show how the correct relativistically covariant behaviour develops for moving mesons once  $v^4$  terms are added to the NRQCD action.

For local current operators we expect the following relativistically covariant behaviour:

$$\begin{aligned} \langle 0 | \bar{\psi} \gamma_5 \psi | \eta_b(\mathbf{p}) \rangle &= \text{constant} & (\text{B1}) \\ \langle 0 | \bar{\psi} \gamma_5 \gamma_0 \psi | \eta_b(\mathbf{p}) \rangle &\propto E_{\eta_b}(\mathbf{p}) \\ \langle 0 | \bar{\psi} \gamma_i \psi | \Upsilon(\mathbf{p}, \lambda) \rangle &\propto \epsilon(\mathbf{p}, \lambda) \end{aligned}$$

where  $\epsilon(\mathbf{p}, \lambda)$  is the  $\Upsilon$  polarisation vector.

To test this for NRQCD we must match NRQCD current operators to continuum ones for a quark-antiquark pair with net spatial momentum. We work simply at tree-level and perform a nonrelativistic expansion of the Dirac bilinear  $\bar{v}(\mathbf{p}) \Gamma u(\mathbf{p})$  in terms of Pauli spinors using

$$\begin{aligned} u(\mathbf{p}) &= \begin{pmatrix} \psi \\ \frac{\boldsymbol{\sigma} \cdot \mathbf{p}}{E+m} \psi \end{pmatrix} \sqrt{\frac{E+m}{2E}} & (\text{B2}) \\ v(\mathbf{p}) &= \begin{pmatrix} \frac{\boldsymbol{\sigma} \cdot \mathbf{p}}{E+m} \chi \\ \chi \end{pmatrix} \sqrt{\frac{E+m}{2E}} \end{aligned}$$

where  $m$  is the quark mass,  $E$ , its energy and we have chosen a nonrelativistic normalisation for the states ( $u^\dagger u = \psi^\dagger \psi = 1$ ). When NRQCD to continuum matching is done for mesons at rest [35] we expand  $\bar{v}(-\mathbf{k}) \Gamma u(\mathbf{k})$  in powers of  $\mathbf{k}$  where  $\mathbf{k}$  is an internal momentum ( $\ll m$ ) for the quarks inside the meson. Higher order terms in  $\mathbf{k}$  become relativistic corrections to the leading order NRQCD current and implemented via derivative operators on the fields. This is the approach taken for the NRQCD vector current in section IID (see eq. (13)). In the case where the meson has momentum  $\mathbf{P}$  we must expand  $\bar{v}(\mathbf{P}/2 - \mathbf{k}) \Gamma u(\mathbf{P}/2 + \mathbf{k})$  in powers of  $\mathbf{P}$  to identify current correction terms coming from this momentum. For simplicity we work to lowest order in  $\mathbf{k}$  i.e. we set  $\mathbf{k}$  to zero. This is sufficient here because the terms in  $\mathbf{P}$  dominate those in  $\mathbf{k}$  when we take a ratio of results between mesons at rest and moving mesons. The terms in  $\mathbf{k}$  will largely cancel because the internal momenta change little, whereas effects from the external momentum,  $\mathbf{P}$ , are only present for moving mesons and are highlighted in such a ratio.

Then to this order :

$$\begin{aligned} \bar{v}(\mathbf{P}) \gamma_5 u(\mathbf{P}) &= \frac{m}{E} \chi^\dagger \psi & (\text{B3}) \\ \bar{v}(\mathbf{P}) \gamma_0 \gamma_5 u(\mathbf{P}) &= \chi^\dagger \psi \\ \bar{v}(\mathbf{P}) \gamma_i u(\mathbf{P}) &= \frac{E+m}{2E} \chi^\dagger \left[ \sigma_i + \frac{\boldsymbol{\sigma} \cdot \mathbf{P}/2}{E+m} \sigma_i \frac{\boldsymbol{\sigma} \cdot \mathbf{P}/2}{E+m} \right] \psi \end{aligned}$$

where  $E \equiv E(\mathbf{P})$ . We see that in the first case the matching generates a simple numerical factor which is a func-

tion of  $\mathbf{P}$  by which to multiply the NRQCD operator. In the second case this factor is simply 1. The third case is more complicated since there is an interplay between momentum components and meson polarisation, but in fact this is exactly what is required to generate the correct sum over polarisation vectors ( $\delta_{ij} + P_i P_j / M^2$ ) in the meson correlation function when two such operators are combined [67].

To test whether and how the factors given in eq. (B3) give the results expected in eq. (B1) we generate NRQCD  $b$  quark propagators and meson correlation functions  $C_{\text{PS},\text{NRQCD}}$  for  $\eta_b$  and  $C_{\text{V},\text{NRQCD}}$  for  $\Upsilon$  using local source and sink operators  $\chi^\dagger \psi$  and  $\chi^\dagger \sigma_x \psi$  respectively. The correlators are generated at zero and non-zero spatial momentum using a random wall source as described for the determination of the kinetic mass in Section IIF. We fit the correlators averaged over configurations to the multi-exponential form given in eq. 6, extracting the ground state amplitude for different momenta,  $c(\mathbf{P})$ , so that:

$$C_{\text{NRQCD}}(t) \stackrel{t \rightarrow \infty}{\simeq} c(\mathbf{P}) c^*(\mathbf{P}) e^{-E_0 t} + \dots \quad (\text{B4})$$

Figure 10 shows results for  $c(\mathbf{P})/c(0)$  for the  $\eta_b$  comparing the NRQCD action we use here that includes terms at  $v^4$ , with the result from just using  $H_0$  along with discretisation corrections to  $H_0$  (i.e. a purely  $v^2$  action) on the fine lattices, set 5. We see very different behaviour – for the full action the amplitude rises linearly with  $P^2$  (as the energy); for the  $v^2$  action it does not.

We now consider the impact of the correction factors in eq. (B3). For the temporal axial current, as indicated in eq. (B3), the factor connecting the NRQCD operator  $\chi^\dagger \psi$  and the Dirac operator is 1. Thus the NRQCD amplitude in this case can be directly compared with the expectation in eq. (B1) since we take a nonrelativistic normalisation for the states. We therefore expect growth of the amplitude according to the ratio of the meson energy to the mass,  $E(\mathbf{P})/M_{\eta_b}$ . Figure 11 shows that indeed, for the full NRQCD action, the temporal axial current matrix element does increase with the energy as it should. It is clear from comparison with Figure 10 that this would not happen for the  $v^2$ -only NRQCD action.

Figure 12 shows equivalent results for the amplitude that can be related to the pseudoscalar current matrix element. Here we have taken

$$c_{\text{rel}}(\mathbf{P}) = c(\mathbf{P}) \frac{m}{\sqrt{P^2/4 + m^2}} \quad (\text{B5})$$

following eq. (B3) for that case. This then results in an amplitude which becomes  $P$ -independent on the fine lattices for the full  $v^4$  NRQCD action, as it should from eq. B1.

For the vector we illustrate the results for the correlator made using  $\chi^\dagger \sigma_x \psi$  at both source and sink. Then the numerical matching factor to convert the NRQCD amplitudes into Dirac amplitudes is given by:

$$c_{\text{rel}}(\mathbf{P}) = c(\mathbf{P}) \left[ \frac{m}{E} + \frac{P_x^2}{E(E+m)} \right] \quad (\text{B6})$$

where  $E = \sqrt{P^2 + m^2}$ . Figure 13 shows the result of applying this matching for  $\Upsilon$  amplitudes as a function of momentum. The results on successively finer lattices again move closer to the expectation from eq. (B1), which in this case is  $\sqrt{1 + P_x^2/M_\Upsilon^2}$ . Note again that this works because the original NRQCD amplitudes  $c(\mathbf{P})$  in the  $\Upsilon$

case behave in a very similar way to that of the  $\eta_b$  amplitudes shown in Figure 10 i.e. with the  $v^2$  only action they are approximately  $P$ -independent (in that case they are indistinguishable from  $\eta_b$  amplitudes since there are no spin-dependent terms in  $H_0$ ) and with the full  $v^4$  action they increase approximately as  $E_\Upsilon$ .

- 
- [1] C. Davies et al. (HPQCD, UKQCD, MILC and Fermilab Lattice Collaborations), Phys.Rev.Lett. **92**, 022001 (2004), hep-lat/0304004.
- [2] C. Davies, PoS **LATTICE2011**, 019 (2011), 1203.3862.
- [3] J. Laiho, E. Lunghi, and R. Van de Water, PoS **LATTICE2011**, 018 (2011), 1204.0791.
- [4] E. J. Eichten and C. Quigg, Phys.Rev. **D52**, 1726 (1995), hep-ph/9503356.
- [5] A. Pineda and A. Signer, Nucl.Phys. **B762**, 67 (2007), hep-ph/0607239.
- [6] N. Brambilla, S. Eidelman, B. Heltsley, R. Vogt, G. Bodwin, et al., Eur.Phys.J. **C71**, 1534 (2011), 1010.5827.
- [7] M. Beneke, Y. Kiyo, P. Marquard, A. Penin, J. Piclum, et al., Phys.Rev.Lett. **112**, 151801 (2014), 1401.3005.
- [8] G. Donald, C. Davies, R. Dowdall, E. Follana, K. Hornbostel, et al. (HPQCD collaboration), Phys.Rev. **D86**, 094501 (2012), 1208.2855.
- [9] D. Becirevic and F. Sanfilippo (2012), 1206.1445.
- [10] C. Davies, K. Hornbostel, A. Langnau, G. Lepage, A. Lidsey, et al., Phys.Rev. **D50**, 6963 (1994), hep-lat/9406017.
- [11] G. T. Bodwin, D. Sinclair, and S. Kim, Phys.Rev. **D65**, 054504 (2002), hep-lat/0107011.
- [12] A. Gray, I. Allison, C. Davies, E. Dalgic, G. Lepage, et al. (HPQCD Collaboration), Phys.Rev. **D72**, 094507 (2005), hep-lat/0507013.
- [13] I. Allison, E. Dalgic, C. T. H. Davies, E. Follana, et al., Phys.Rev. **D78**, 054513 (2008), 0805.2999.
- [14] C. McNeile, C. Davies, E. Follana, K. Hornbostel, and G. Lepage (HPQCD Collaboration), Phys.Rev. **D82**, 034512 (2010), 1004.4285.
- [15] G. P. Lepage, L. Magnea, C. Nakhleh, U. Magnea, and K. Hornbostel, Phys.Rev. **D46**, 4052 (1992), hep-lat/9205007.
- [16] R. Dowdall, B. Colquhoun, J. O. Daldrop, C. T. H. Davies, et al. (HPQCD Collaboration), Phys.Rev. **D85**, 054509 (2012), 1110.6887.
- [17] A. Lee, C. J. Monahan, R. R. Horgan, et al. (HPQCD Collaboration), Phys.Rev. **D87**, 074018 (2013), 1302.3739.
- [18] S. Dawson, A. Gritsan, H. Logan, J. Qian, C. Tully, et al. (2013), 1310.8361.
- [19] G. P. Lepage, P. B. Mackenzie, and M. E. Peskin (2014), 1404.0319.
- [20] A. Bazavov et al. (MILC Collaboration), Phys.Rev. **D87**, 054505 (2013), 1212.4768.
- [21] E. Follana et al. (HPQCD Collaboration), Phys.Rev. **D75**, 054502 (2007), hep-lat/0610092.
- [22] A. Hart, G. von Hippel, and R. Horgan (HPQCD Collaboration), Phys.Rev. **D79**, 074008 (2009), 0812.0503.
- [23] T. Hammant, A. Hart, G. von Hippel, R. Horgan, and C. Monahan, Phys.Rev. **D88**, 014505 (2013), 1303.3234.
- [24] R. Dowdall, C. Davies, R. Horgan, C. Monahan, and J. Shigemitsu (HPQCD Collaboration), Phys.Rev.Lett. **110**, 222003 (2013), 1302.2644.
- [25] J. Daldrop, C. Davies, and R. Dowdall (HPQCD Collaboration), Phys.Rev.Lett. **108**, 102003 (2012), 1112.2590.
- [26] R. Dowdall, C. Davies, T. Hammant, and R. Horgan (2013), 1309.5797.
- [27] R. Dowdall, C. Davies, T. Hammant, and R. Horgan (HPQCD Collaboration) (2012), 1207.5149.
- [28] C. Davies, E. Follana, I. Kendall, G. P. Lepage, and C. McNeile (HPQCD Collaboration), Phys.Rev. **D81**, 034506 (2010), 0910.1229.
- [29] J. Beringer et al. (Particle Data Group), Phys. Rev. **D86**, 010001 (2012).
- [30] E. B. Gregory, C. T. Davies, I. D. Kendall, J. Koponen, K. Wong, et al. (HPQCD Collaboration), Phys.Rev. **D83**, 014506 (2011), 1010.3848.
- [31] J. Erler, Phys.Rev. **D59**, 054008 (1999), hep-ph/9803453.
- [32] G. Adams et al. (CLEO Collaboration), Phys.Rev.Lett. **94**, 012001 (2005), hep-ex/0409027.
- [33] J. Rosner et al. (CLEO Collaboration), Phys.Rev.Lett. **96**, 092003 (2006), hep-ex/0512056.
- [34] D. Besson et al. (CLEO Collaboration), Phys.Rev.Lett. **98**, 052002 (2007), hep-ex/0607019.
- [35] A. Hart, G. von Hippel, and R. Horgan, Phys.Rev. **D75**, 014008 (2007), hep-lat/0605007.
- [36] B. Jones and R. Woloshyn, Phys.Rev. **D60**, 014502 (1999), hep-lat/9812008.
- [37] C. Davies et al. (UKQCD Collaboration), Phys.Rev. **D58**, 054505 (1998), hep-lat/9802024.
- [38] K. Chetyrkin, J. H. Kuhn, and C. Sturm, Eur.Phys.J. **C48**, 107 (2006), hep-ph/0604234.
- [39] R. Boughezal, M. Czakon, and T. Schutzmeier, Phys.Rev. **D74**, 074006 (2006), hep-ph/0605023.
- [40] A. Maier, P. Maierhofer, and P. Marquard, Phys.Lett. **B669**, 88 (2008), 0806.3405.
- [41] A. Maier, P. Maierhofer, P. Marquard, and A. Smirnov, Nucl.Phys. **B824**, 1 (2010), 0907.2117.
- [42] Y. Kiyo, A. Maier, P. Maierhofer, and P. Marquard, Nucl.Phys. **B823**, 269 (2009), 0907.2120.
- [43] M. Czakon and T. Schutzmeier, JHEP **0807**, 001 (2008), 0712.2762.
- [44] J. H. Kuhn, M. Steinhauser, and C. Sturm, Nucl.Phys. **B778**, 192 (2007), hep-ph/0702103.
- [45] G. P. Lepage et al., Nucl. Phys. Proc. Suppl. **106**, 12 (2002), hep-lat/0110175.
- [46] C. Davies, C. McNeile, E. Follana, G. Lepage, H. Na, et al. (HPQCD Collaboration), Phys.Rev. **D82**, 114504 (2010), 1008.4018.
- [47] C. McNeile, C. Davies, E. Follana, K. Hornbostel, and G. Lepage, Phys.Rev. **D86**, 074503 (2012), 1207.0994.
- [48] K. Chetyrkin, J. Kuhn, A. Maier, P. Maierhofer, P. Marquard, et al., Phys.Rev. **D80**, 074010 (2009), 0907.2110.

- [49] B. Chakraborty, C. Davies, G. Donald, R. Dowdall, J. Koponen, et al. (2014), 1403.1778.
- [50] S. Bodenstein, C. Dominguez, and K. Schilcher, *Phys.Rev.* **D85**, 014029 (2012), 1106.0427.
- [51] C. Davies, B. Colquhoun, B. Galloway, G. Donald, J. Koponen, et al., *PoS LATTICE2013*, 438 (2013), 1312.5874.
- [52] K. Chetyrkin, B. A. Kniehl, and M. Steinhauser, *Nucl.Phys.* **B510**, 61 (1998), hep-ph/9708255.
- [53] I. Adachi et al. (Belle Collaboration), *Phys.Rev.Lett.* **110**, 131801 (2013), 1208.4678.
- [54] K. Hara et al. (Belle collaboration), *Phys.Rev.* **D82**, 071101 (2010), 1006.4201.
- [55] B. Aubert et al. (BaBar Collaboration), *Phys.Rev.* **D81**, 051101 (2010), 0912.2453.
- [56] B. Aubert et al. (BaBar Collaboration), *Phys.Rev.* **D77**, 011107 (2008), 0708.2260.
- [57] G. Donald, C. Davies, J. Koponen, and G. Lepage (HPQCD Collaboration) (2013), 1311.6669.
- [58] G. Donald, C. Davies, J. Koponen, and G. Lepage (HPQCD Collaboration), *Phys.Rev.Lett.* **112**, 212002 (2014), 1312.5264.
- [59] R. Dowdall, C. Davies, G. Lepage, and C. McNeile, *Phys.Rev.* **D88**, 074504 (2013), 1303.1670.
- [60] A. Bazavov et al. (Fermilab Lattice and MILC Collaborations) (2014), 1407.3772.
- [61] E. Follana, C. Davies, G. Lepage, and J. Shigemitsu (HPQCD Collaboration), *Phys.Rev.Lett.* **100**, 062002 (2008), 0706.1726.
- [62] B. Chakraborty, C. T. H. Davies, B. Galloway, et al. (HPQCD Collaboration) (2014), 1408.4169.
- [63] N. Carrasco, P. Dimopoulos, R. Frezzotti, V. Gimnez, P. Lami, et al. (2013), 1311.2837.
- [64] C. Davies, K. Hornbostel, A. Langnau, G. Lepage, A. Lidsey, et al., *Phys.Rev.Lett.* **73**, 2654 (1994), hep-lat/9404012.
- [65] A. X. El-Khadra, A. S. Kronfeld, and P. B. Mackenzie, *Phys.Rev.* **D55**, 3933 (1997), hep-lat/9604004.
- [66] C. Bernard et al. (Fermilab Lattice Collaboration, MILC Collaboration), *Phys.Rev.* **D83**, 034503 (2011), 1003.1937.
- [67] J. J. Dudek, R. G. Edwards, and D. G. Richards, *Phys.Rev.* **D73**, 074507 (2006), hep-ph/0601137.